Instituto Nacional de Astrofísica, Optica y Electrónica.

LIQUID CRYSTAL REORIENTATION INDUCED BY PHOTOISOMERIZATION AND ITS APPLICATIONS IN IMAGE PROCESSING

Por

Rosario G. Porras Aguilar

Tesis sometida como requisito parcial para obtener el grado de Doctora en Ciencias en la especialidad de Óptica en el Instituto Nacional de Astrofísica, Óptica y Electrónica.

Supervisada por:

Dr. Rubén Ramos García, INAOE
Dr. Julio César Ramírez San Juan, INAOE

Tonantzintla, Puebla.

13 de agosto de 2009

Liquid crystal reorientation induced by photoisomerization and its applications in image processing

M. C. Rosario Porras Aguilar

Tesis sometida como requisito parcial para obtener el grado de Doctora en Ciencias en la especialidad de Óptica en el Instituto Nacional de Astrofísica Óptica y Electrónica.
Supervisada por

Dr. Rubén Ramos García

Dr. Julio César Ramírez San Juan

Abstract

Dye doped liquid crystals are interesting materials which present a *colossal* optical nonlinearity ($n_2 = 10^3 cm^2/W$) [1]. This dissertation is focused on the effects that contribute to the reorientation of the liquid crystal molecules induced by the dye photoanchoring to the substrate, and which are responsible for the formation of permanent gratings. It was found that small changes in the substrate due to the dye anchoring, leads to large changes in the bulk liquid crystal reorientation.

In addition, the outstanding characteristics of this material, which include low power illumination requirements, among others, are exploited in phase contrast microscopy [2]. An inversion in the image contrast of a known phase object has been observed by changing the polarization from extraordinary to ordinary. So far, the minimum phase change resolvable is $\lambda/8$ at $633nm$. This method can be implemented in real time, and the contrast can be tuned by adjusting the intensity and polarization of the illumination beam, temperature and electric fields.

Acknowledgements

I would like to thank the many people who have helped and supported me during my studies leading to this dissertation. First of all, I want to express my highest gratitude to my advisors, Dr. Ruben Ramos García and Dr. Julio Cesar Ramírez San Juan, without whom this work would have been impossible to accomplish. I greatly appreciate his support and guidance given to me throughout my years at the National Institute for Research in Astrophysics, Optics and Electronics.

I would like also to thank my committee members: Doctors Luis Arroyo, Alejandro Cornejo, David Iturbe, David Sánchez, and Carlos Treviño for their helps and for providing invaluable suggestions and comments to this dissertation.

I need to thank the support given to this dissertation by the Mexican Science Council (CONACyT) and by the Puebla Science Council (CONCyTEP).

In addition, I wish to thank my family for their continual support and cheering through the years.

I consider my self very lucky to have the best friends one can have. Thank you all guys for being there!

Finally, I would like to thank the facilities given by the National Institute for Research in Astrophysics, Optics and Electronics. This institute is what it is because of its people. I am very greatful with all of them, including managers, researchers, secretaries, students, technicians, general workers, thank you all.

Contents

List of Figures

Chapter 1

Introduction

1.1 Background

The discovery of novel nonlinear optical materials is an atracttive research field. Its ambitious goal is the replacement of the electronic or electro-optical devices for all-optical systems [3]. However, these devices require high powers to work properly what makes impossible their implementation for real-time applications. Therefore, large nonlinear materials are required for photonic applications where it is possible to make use of weaker and unfocused lasers.

Liquid crystals (LCs) exhibit such a kind of optical nonlinearity. Their optical properties have been broadly studied over the last three decades and applied in different fields. Nowadays, LCs have been exploited in the display industry, and they are used to construct spatial light modulators (SLMs). In addition, they have been employed in real-time image processing and in optical computing applications [4]. LCs are also used to fabricate optical switching devices, highly sensitive temperature sensors and thermographical devices, among many other usages [5].

The surge of the nonlinear optical properties of LCs research began in 1980, when Zeldovich *et al*. [6] reported the observation of giant optical nonlinearity in transparent LCs ($n_2 = 10^{-5} cm^2/W$) caused by collective molecular reorientation of this material, representing at that time the largest nonlinearity ever achieved. Ten years later, Janossy et al. [7] noted that nonlinear effect can be enhanced by an additional

torque exerted by anthraquinone dyes, obtaining $n_2 = 10^{-3} cm^2/W$. After some years, Khoo *et al*. [8] reported even larger values for $n_2 \approx 1 cm^2/W$ by doping the liquid crystal 5CB with a small amount of the azo-dye methyl red (MR) [9]. It was interpreted as a photorefractive-like effect based on the photo-induced space-charge field generated by the spatial modulation of the conductivity and the dielectric anisotropy of the liquid crystal. Recently, Lucchetti *et al*. [1] obtained a nonlinear refractive index of $n_2 \approx 10^3 cm^2/W$ in randomly-oriented thin liquid crystal cells. The authors called this effect as *colossal* nonlinearity. The origin of the nonlinearity was attributed to a surface-induced nonlinear effect, particularly photoadsorption of the dye to the glass substrate, which produced a volumetric reorientation when the anchoring conditions of the dye are affected by light [10].

Unfortunately, azo-dye methyl red doping presents a side effect: the permanent anchoring of the dye molecule to the substrate. This effect can be undesirable for some applications (displays, SLM, etc.), while in others, such as optical memories, holography, etc., it is possible to take advantage of the molecular anchoring [11]. In this dissertation these phenomena are studied in order to understand and control the mechanisms present during the photoisomerization.

On the other hand, the prominent characteristics of dye doped liquid crystals (DDLCs), (low power requirements, refractive index dependent on intensity and polarization, among others) suggest that this material may be the best candidate for nonlinear optical phase contrast applications. This technique requires a specific and localized refractive index modulation (at the Fourier plane of the system) to convert phase information into intensity changes. The conventional phase contrast microscope was developed by Frits Zernike, for which he obtained the Nobel Prize in 1953 [12]. Nevertheless, this device suffers for the difficulties of the phase filter construction and for the alignment of this filter in the optical system. However, the use of a nonlinear material as a Zernike filter solves this problem i.e., its refractive index dependent on intensity allows the self phase modulation, and it is self aligned. Concerning the DDLC, one of its most remarkable advantages is the possibility to tune the contrast of the acquired images by controlling the light's polarization of illumi-

nation. This is a noteworthy advantage because it is not available in other standard nonlinear materials, and makes them promising for real time applications.

1.2 Objective of the Thesis

This section is focused on describing with detail the general and specific objectives of this research.

- An important goal of this dissertation is to study and elucidate the molecular mechanisms involved in the photoinduced optical nonlinearity present in azo-dye-doped nematic liquid crystal (4-pentyl-4'-ciano-biphenyl, 5CB). The presence of dye molecules has an enormous contribution to the nonlinear optical enhancement behavior. However, the interest is focused on the molecular interactions between the material and the cell substrate. To achieve this aim, the following specific goals need to be accomplished:
  - To describe and control the mechanism responsible for the formation of permanent gratings on azo-dye doped liquid crystals.
  - To perform pump-probe configuration experiments on two chemically similar azo-dyes used to dope the nematic LC 5CB (methyl red and methyl yellow) in order to characterize the photoinduced optical nonlinearities.
  - To compare the nonlinear optical behavior of dye-doped nematic LC with both dyes.
  - To analyze and clarify the anisotropic behavior of the gratings recorded on DDLC cells upon a polarized probe beam.
  - To measure the response and relaxation time of the DDLC system as function of intensity and polarization of the pump beam.

As mentioned before, methyl red dye shows molecular adsorption to the substrate, but the methyl yellow does not present any permanent photoadsorption. The only chemical structure difference between these dyes is the acid group position in the phenyl ring (i.e. 2'-COOH on MR). Our hypothesis is that this acid group is involved

in the dye anchoring on the substrate. Therefore, the analysis of the measurements as well as the study of the dye contribution to the photoalignment of LC molecules are needed to elucidate this process.

Besides, in order to take advantage of the extraordinary nonlinearity of DDLCs in the phase contrast technique (where the phase modulation is crucial) it is necessary:

- To find the dependence of the phase change induced by the cell as function of the intensity and polarization's beam. To accomplish this aim the following is needed:
  - To measure transmission values of the sample for low and saturation intensities as function of polarization. Such values are related with the phase change induced by a DDLC cell.

References [13, 14] report strong dependence of the sign of the nonlinearity of DDLCs on polarization's illumination. For this reason, it is expected to find an important contribution in the phase change due to polarization. Actually, based on this fact, the implementation of a phase contrast microscope using a DDLC cell as a Zernike filter is purposed. According to that, the next goals are:

- To demonstrate that a DDLC cell with molecular planar alignment can be employed as a nonlinear filter in a phase contrast microscope. Even more, it is important to prove that its intensity and polarization dependence solve common alignment difficulties, while allowing real-time contrast tuning of the images. Thus, the specific goals are needed:
  - To implement an image forming system placing a DDLC cell at the Fourier plane in order to obtain a phase contrast microscope.
  - To evaluate the performance of this cell as a Zernike filter comparing the contrast of the images for different known thick phase objects.
  - To characterize the image contrast as function of intensity and polarization illumination.
  - To prove that it is possible to adjust the contrast in the images for real-time applications by rotating the beam's polarization.

Taking into consideration the outstanding features of DDLC, it is expected to achieve high contrasted images and exciting applications for the nonlinear phase contrast based on the employment of this material.

1.3 Outline

The content of this document is organized as follows. Chapter 2 gives the theoretical basis of this research work. The first section contains a review of liquid crystals and its nonlinear optical properties. The basic features and classification of liquid crystals are given. In addition, the liquid crystalline phases, the order parameter and the liquid crystal anisotropy are defined. The nonlinear optical properties of transparent liquid crystals and the Janossy effect in dye doped liquid crystals are defined. This section ends with a concise description of the grating diffraction formation and Z-scan as techniques to measure optical nonlinearities. The second section of this chapter includes the classical and a generalized approach of the phase contrast theory. A general expression for the image contrast for phase filtering is given. Chapter 2 concludes with a review of the employment of a nonlinear material as Zernike filter.

The experimental results related with the understanding of the photoisomerization of azo dye molecules as dopants of LCs are presented in Chapter 3. Sections 2 and 3 report the study of the molecular mechanisms which gives rise to the dye anchoring on the substrate and its induced alignment over the LC molecules. These results employs the grating diffraction formation in order to measure the nonlinear contribution over the sample. The following section shows the anisotropy of the sample for low intensity (linear regimen), and section 5 presents the discussion related with the dynamics of the response and relaxation time of the material. The last section of Chapter 3 describes the experiments in order to obtain an expression for the phase change as function of intensity and polarization illumination.

Chapter 4 shows the contrasted images obtained by using a dye doped liquid crystal planar cell as nonlinear filter in the phase contrast technique. The performance of the technique is demonstrated by showing the image contrast of known thick phase objects and for different illumination intensities. The results confirmed that the phase

change in the LC sample, and hence the image contrast, can be controlled by rotating the beam's polarization. This chapter also includes the images of intriguing edge enhancement of a $4.8\pi rad$ thickness phase object, as well as the high contrasted images acquired for living organisms in real time.

Finally, Chapter 5 gives a discussion of the contribution of this dissertation. The aims of this research work are reviewed and the perspectives of this work are analyzed.

Chapter 2

Theoretical Basis

The objective of this chapter is to provide the basic theory involved in this research work. A general background on the physical properties of liquid crystals and on their nonlinear optical behavior is presented. In addition, one section of this chapter is focused on the main phase contrast microscopy concepts. The nonlinear version of the Zernike microscope is also reviewed and the use of a dye-doped-liquid crystal cell as a Zernike filter is analyzed.

2.1 Basic Review of Azo-Dye-Doped Liquid Crystals and their Nonlinear Optical Behavior

The first observations of liquid crystalline or *mesomorphic* behavior were made in 1888 by Reinitzer and Lehmann [15]. When Reinitzer found two melting points in some cholesterol samples (at 145.5° C and 178.5° C), he sent them to Lehmann who was studying crystallization properties of some substances. Lehmann found that even though cholesterol flows like a liquid when observed under a cross-polarized microscope, it has some similarities with crystals. At that time, he called them flowing crystals but later used the term *liquid crystals*.

2.1.1 General description of liquid crystals

Liquid crystals are materials that exhibit one or more intermediate phase(s) between crystalline solid and isotropic liquid phases. The molecules in a crystal are ordered whereas in a liquid they are not. The existing order in a crystal is usually both positional and orientational, i.e., the molecules are constrained both to occupy specific sites in a lattice and to point their molecular axes in specific directions. Quite the opposite, the molecules in liquids are randomly diffused throughout the sample container with the molecular axes tumbling wildly [5]. Likewise, in intermediate phases (called mesophases) liquid crystals retain the ability to flow like ordinary liquid, but also possess long-range orientational order (whether or not molecules are pointing in the same direction). Some LCs may also have positional order as well (whether or not molecules are arranged in any sort of ordered lattice).

Liquid crystals have an important characteristic which they share with solids: they are *anisotropic* substances. This anisotropy manifests itself in many physical properties, i.e., optical, mechanical, electrical. When external fields (electric or magnetic) are applied to a liquid crystal, the field will align the anisotropic molecules because of the interaction with the permanent or induced dipoles of the molecules. As a consequence, a molecular redistribution also occurs due to the interaction among the induced dipoles. The reorientation and redistribution of molecules give rise to a change of the molecular polarizabilities that depend on the field strength and may lead to effects such as nonlinear scattering or nonlinear birefringence [16].

2.1.2 Chemical structure of liquid crystals

The typical chemical structure of a liquid crystal comprises a side chains R and a terminal group R' at the beginning and at the end of the molecule, respectively. Two or more aromatic rings, A and A' in the middle, are connected by linkage groups X (See Fig.2.1) [17].

As side chain and terminal groups one can find alkyl, alkoxy, and others. The Xs of the linkage groups are simple bonds or groups as stilbene, ester, tolane, azoxy, and others. The names of liquid crystals are normally related with the linkage group.

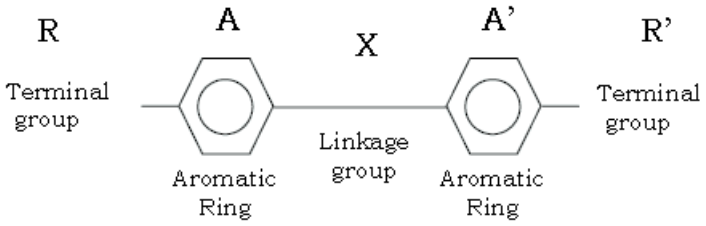

Figure 2.1: Molecular structure of a typical liquid crystal molecule.

The liquid crystal employed in our experiments is the nematic 4-pentyl-4'-cyano-biphenyl, known by the abbreviation 5CB. The chemical representation of 5CB is shown in figure 2.2.

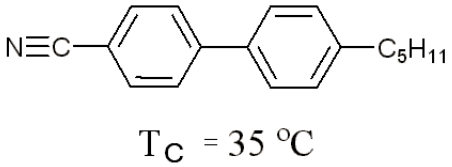

Figure 2.2: Molecular structure of 5CB nematic liquid crystal molecule. T_C is the transition temperature from nematic to isotropic phase, also known as cleanning temperature.

2.1.3 Classification of liquid crystals

One can classify liquid crystals according to the physical parameters controlling the existence of the liquid crystalline phases. By considering these parameters, three distinct types of liquid crystals can be distinguished: *lyotropic*, *polymeric* and *thermotropic*.

Lyotropic liquid crystals are obtained when an appropriate concentration of a material is dissolved in some solvent. The most important variable to control the existence of the liquid crystalline phase is the concentration of the dissolution. Polymerics, likewise, can be described as polymer versions of the basic monomers on which

LC's behavior is based (discussed in Section 2.1.2). There are three common types of polymers characterized by the degree of flexibility. The most flexible is the *vinyl* type, while the *Dupont Kevlar* polymer is semirigid and the *polypeptide chain* is the most rigid [17]. When transitions to the mesophases in LCs are obtained by purely thermal processes, they are called thermotropic LCs. The experiments reported in this dissertation are based on thermotropic ones, therefore the next subsection is focused on their optical properties.

2.1.3.1 Thermotropic liquid crystals

Thermotropic liquid crystals are the most widely used and extensively studied due their linear as well as nonlinear optical properties [17]. The change in the phase from crystalline solid to liquid crystal appears when the temperature is raised above its melting point (T_M). If the temperature is further increased to the clearing point (T_C), the phase changes from liquid crystalline to isotropic liquid (Fig. 2.3).

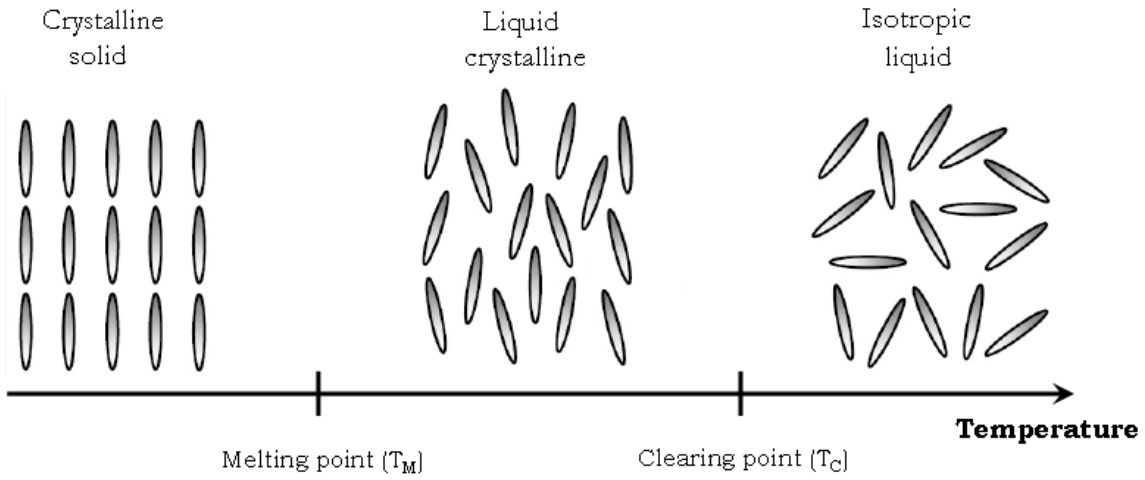

Figure 2.3: Mesophases of thermotropic liquid crystal as a function of temperature: (left) solid state, (middle) liquid crystal and (right) isotropic liquid.

There are three main classes of thermotropic liquid crystals classified by their orientational and positional order: *nematic*, *cholesteric* or *chiral nematic* , and *smectic*. Nematic molecules have only orientational order throughout the bulk, there exists no positional order. Thus, the molecules flow and are randomly distributed as in a

liquid, but they all point in the same direction. Most of the nematic phases are uniaxial, Fig.2.4(a) . Likewise, cholesterics resemble nematic liquid crystals in all physical properties except that the molecules tend to align in a helical manner Fig.2.4(b). The twist may be right-handed or left-handed depending on the molecular conformation. The spiral arrangement of the molecules in the cholesteric is responsible for its unique optical properties, i.e., the selective reflection of circularly polarized light and a rotatory power about thousand times greater than that of an ordinary optically active substance [15]. The smectic phase has orientational order but also certain degree of positional order. Several forms of smectic phases have been discovered and labeled by a letter from the alphabet. Currently, smectic A to smectic C phases have been found. They are characterized by their tilt angle (with respect to the plane normal) and packing formation, see Fig. 2.4(c). In both the smectic A and smectic C phases, the molecules are randomly diffused within each plane. No positional order exists within each plane, so in a sense the positional order is in one dimension only. However, other smectic liquid crystals phases exist in which the molecules are somewhat ordered within each plane.

2.1.4 Order in liquid crystals

Liquid crystals in the isotropic phase (different from liquids) can possess a short range order. In this phase, the molecules within a short distance of one another are correlated by intermolecular interactions. Therefore the physical and optical behavior of liquid crystals can be described in two different ways: the ordered and the disordered. The ordered (nematic) phase can be characterized by a long range order (not complete) and crystalline-like physical properties and the disordered (isotropic) phase by a short range order. Both order parameters show critical dependences near the phase transition temperature T_C from nematic to isotropic phase or the opposite direction.

In the most simple liquid crystal phase, one molecular axis tends to point along a preferred direction. This preferred direction is called the *director* and is denoted by the unit vector **n**. In order to specify the amount of orientational order in such a

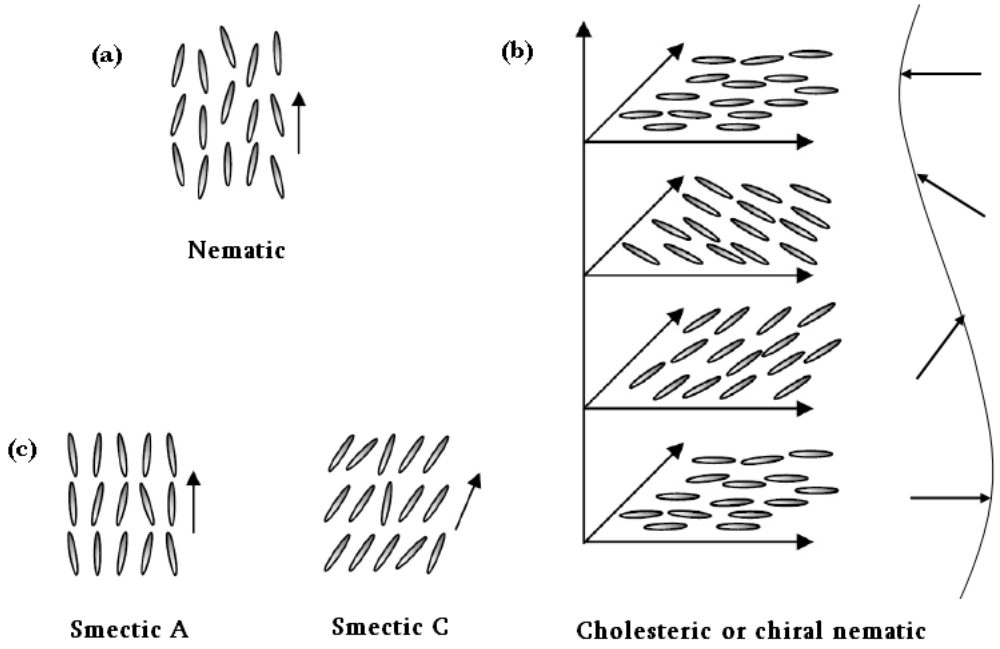

Figure 2.4: Three different types of thermotropic liquid crystals: nematic, cholesteric and smectic. Arrows show the preferential molecular orientation.

liquid crystal phase, an order parameter S is defined. Since the LC molecules are not fixed, S can be described in many ways. The most useful formulation is to find the average of the second Legendre polynomial P_2, as defined in Eq.2.1.

$$S = \langle P_2(\cos\theta)\rangle = \frac{1}{2}\left\langle 3\cos^2\theta - 1\right\rangle . \tag{2.1}$$

This quantity can be interpreted as an averaged quantity related with the angle θ between **n** and every axis molecule. See Fig.2.5.

In equation2.1, S goes from 0 to 1, for disordered to ordered phases, respectively. Typical values for the order parameter are between 0.3 and 0.9 [18]. S can be measured by different methods. Usually it is determined by a macroscopic property of the liquid crystal phase measurement. Some examples of these properties are diamagnetism, optical birefringence, nuclear magnetic resonance, and Raman scattering [19].

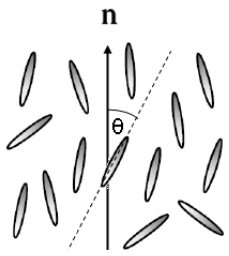

Figure 2.5: Geometry used for defining order parameter. **n** represents the director axis and θ the angle between the director and the molecule axis of the liquid crystal. In nematics, the director has the symmetry $\mathbf{n} \rightarrow -\mathbf{n}$ and identifies a single direction.

The average of fourth Legendre polynomial can also be used to define orientational order parameter. This expression is shown in Eq.2.2. However, measuring P_4 order parameter is more difficult than measuring S, but it can be achieved by using Raman scattering, X-ray scattering, neutron scattering, and spin resonance.

$$\langle P_4(cos(\theta))\rangle = \frac{1}{8}\left\langle 35\ cos^4\theta - 30\ cos^2\theta + 3\right\rangle . \tag{2.2}$$

In particular studies or applications of liquid crystal samples, long-range orientational order can be induced. It can be achieved by imposing particular boundary conditions at the confining surfaces of the cell, called *anchoring conditions*. Typical anchoring conditions for a liquid crystal sample may be either homeotropic (**n** orthogonal to the confining plates) or planar (**n** parallel to the confining plates) as shown in Fig.2.6.

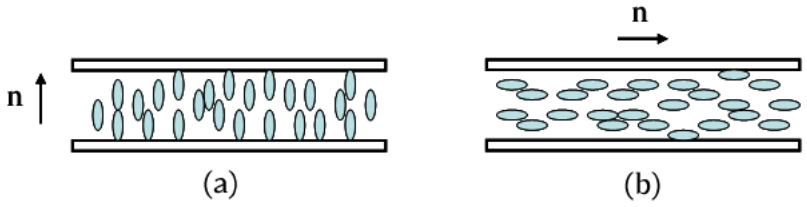

Figure 2.6: Liquid crystal anchoring configurations: (a) homeotropic; (b) planar.

The order existing in the liquid crystalline phases destroys the isotropy and induces anisotropy in the system. The macroscopic anisotropy is observed because the

molecular anisotropy responsible for this property does not average out to zero as is the case in an isotropic phase. Under some circumstances it is possible to photoinduce molecular reorientation and thus, the anisotropy of the material can be controlled.

2.1.5 Anisotropic physical properties

As mentioned before, the molecular reorientation and redistribution gives origin to nonlinear optical phenomena. These effects are observed in materials which are isotropic but are constituted by anisotropic molecules. Liquid crystals present a peculiar characteristic: they are not only constituted of anisotropic molecules but they also keep this anisotropy on a macroscopic scale [16]. This anisotropy is manifested in many physical properties. Actually, due to this characteristic it is possible to achieve nonlinear optical behavior. In the following, a brief discussion of the optical and dielectric anisotropic properties is given.

2.1.5.1 Optical anisotropy: the refractive index

The liquid crystals are optically anisotropic materials, i.e., the propagation velocity of light waves in this medium is no longer uniform but is dependent upon the direction and polarization of the light waves transversing the material. As a consequence, the material is found to possess different refractive indices in different directions [19]. The optical anisotropy (or birefringence), defined by Eq. 2.3, depends on the electric field intensity, wavelength, temperature, polarization, among others.

$$\Delta n = n_e - n_o = n_{\parallel} - n_{\perp}, \tag{2.3}$$

where n_e and n_0 are the extraordinary and ordinary refractive indices, respectively. $n_{\parallel}$ and $n_{\perp}$ are the parallel and perpendicular components of the refractive indices to the long molecular axis. See Fig. 2.7 For rod-like molecules $n_{\parallel} > n_{\perp}$; therefore Δn is positive.

There are many methods to determine Δn i.e., the pump-probe geometry, elipsometry, among others.

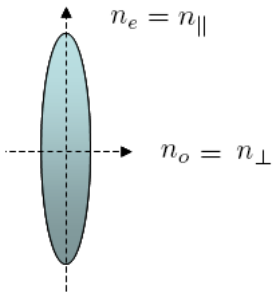

Figure 2.7: Refractive indices of a single liquid crystal molecule. $n_e = n_{\|}$ is the extraordinary refractive index given along the longest molecular axis, $n_0 = n_{\perp}$ is the ordinary refractive index given along the shortest molecular axis.

2.1.5.2 Dielectric anisotropy: the dielectric permittivity

When a dielectric material is affected by an electric field, positive charges move toward the applied field direction, while the negative ones move to the opposite direction. These movements induce an electric dipole moment in the material. Thus, an applied electric field induces a macroscopic polarization of the dielectric medium. For low intensity, the polarization is proportional to the amplitude of the electric field **E**

$$\mathbf{P} = \chi \mathbf{E}, \tag{2.4}$$

where χ is the electric susceptibility of the medium. Under these conditions the displacement **D** is proportional to **E**,

$$\mathbf{D} = \varepsilon \mathbf{E}, \tag{2.5}$$

where $\varepsilon = 1 + 4\pi\chi$ is the dielectric constant or the relative electric permittivity. If the dielectric medium is isotropic and uniform, ε is independent of position and is described as $\varepsilon = n_0^2$, where n_0 is the refractive index of the medium [20]. This description is valid only as long as the polarization is linearly dependent of the electric field.

In the case of nematic liquid crystals, they can be treated as uniaxial molecules. Since the axis of the material is defined by the director **n**, the dielectric constant becomes a tensor of the form [20, 21]

$$\underline{\varepsilon} = \begin{pmatrix} \varepsilon_\perp & 0 & 0 \\ 0 & \varepsilon_\perp & 0 \\ 0 & 0 & \varepsilon_\parallel \end{pmatrix}, \tag{2.6}$$

where $\varepsilon_\perp$ and $\varepsilon_\parallel$ are the dielectric constants perpendicular and parallel to **n**, respectively. The dielectric anisotropy is defined then as the difference between both constants, $\Delta\varepsilon = \varepsilon_\parallel - \varepsilon_\perp$. This quantity measures the difference of polarizability of the molecules along different directions with respect to the applied field [22]. — Liquid crystal molecules tend to orient themselves either parallel or orthogonal to the direction of the applied field, depending on the sign of their dielectric anisotropy. If $\Delta\varepsilon > 0$, molecules tend to orient parallel to the applied field. Otherwise, if $\Delta\varepsilon < 0$ molecules orient perpendicular to the applied field. However, for high-frequency fields all known liquid crystals are characterized by positive $\Delta\varepsilon$ [17].

Under the action of light an optical electric field is applied, thus an optical torque acting on the liquid crystal molecules is developed. This subject gives rise to the large optical nonlinearity in LCs and is analyzed in the following section.

2.1.6 The optical nonlinearity of transparent nematic liquid crystals

The phenomenon of photoinduced molecular reorientation of absorbing nematic liquid crystals has been widely analyzed by many authors. See for example: [6, 23]. This interesting mechanism is originated from the interaction between the optical field and the induced polarization over an anisotropic medium.

According to Jánossy *et al*. [24], if the induced material polarization is not parallel to the optical electric field, a net torque per unit volume acting on the medium is developed. In most materials, the effect of the optical torque is hardly detectable even when generated by the intense light of a pulsed and focused laser beam. However, in nematic liquid crystals the optical torque can easily induce a large change of the molecule average orientation. This effect, known as photoinduced molecular reori-

entation, is at the basis of the LC giant optical nonlinearity, and has been object of extensive studies in the last decades.

2.1.6.1 The optical nonlinearity

For high light intensities, all materials show a nonlinear optical behavior. In Eq.2.4, it is assumed that the polarization is a linear function of the electric field. However, as the case may be, for very high light intensities, higher order terms of 2.4 need to be taken into consideration as shown in Eq.2.7,

$$P_i = \sum_j \chi_{ij}^{(1)} E_j + \sum_{jk} \chi_{ijk}^{(2)} E_j E_k + \sum_{jkl} \chi_{ijkl}^{(3)} E_j E_k E_l + \cdots . \tag{2.7}$$

Here the χ's are tensors of various orders and represent the nonlinear coefficients [25]. Since in the experiments only one component of the electric field and of the polarization is important, a simplified expression can be written as

$$P = \chi^{(1)} E + \chi^{(2)} E^2 + \chi^{(3)} E^3 + \cdots . \tag{2.8}$$

The first term $\chi^{(1)}$ is associated with the common linear polarization and thus, with the refractive index of matter. $\chi^{(2)}$ is different from zero only for some special types of crystals (noncentrosymmetric mediums), while $\chi^{(3)}$ is the responsible for the *Kerr* effect. For centrosymmetric medium, the final equation for the nonlinear polarization can be written as

$$P = [\chi^{(1)} + \chi^{(3)} E^2] E \equiv \chi_{eff} E. \tag{2.9}$$

In this equation χ_{eff} represents the effective susceptibility of the medium and is proportional to the light intensity ($I \propto E^2$). Since the refractive index depends on χ_{eff}, it is not longer a constant, but depends linearly on the intensity light

$$n \approx n_0 + n_2 I, \tag{2.10}$$

where n_0 is the linear refractive index and the coefficient n_2 is a measure of the nonlinearity of the medium. Such a kind of response (n depends linearly on the intensity), is know as optical Kerr effect.

The optical Kerr effect has been observed in liquids, solids and also gases, for example: benzene, chloroform, among others [26]. This effect gives rise to many phenomena, such as, self-focusing [16], self-phase-modulation, optical solitons [25], phase conjugation, among others. For glasses, the typical order of magnitude of the nonlinear coefficient is $n_2 = dn/dI \approx 10^{-14} cm^2/W$.

For transparent liquid crystals the nonlinear coefficient is $n_2 = 10^{-5} cm^2/W$; i.e., nine orders of magnitude larger than in glasses. For this reason, the liquid crystal nonlinearity is called *giant* nonlinearity. However, it is mandatory to mention that the nonlinearity present in liquid crystals is not strictly a Kerr nonlinearity, and it does not strictly obey Eq.2.10 because is orientational. Thus, this value is not a true material property but is actually geometry dependent, i.e., varying with the sample thickness and the beam incident angle [3].

2.1.6.2 The physical mechanism of nonlinearity

The physical mechanism that leads the response of nematic liquid crystals is similar to the well-known electro-optical response of nematic liquid crystals, and can be explained as the result of four steps [3, 17, 23, 27].

1. The optical electric field **E** induces a polarization **P** that is not parallel to the field (due to dielectric anisotropy) Fig. 2.8:

$$\mathbf{P} = \varepsilon_0 (\varepsilon_\perp - 1)\mathbf{E} + \Delta\varepsilon(\mathbf{E}\cdot\mathbf{n})\mathbf{n} \tag{2.11}$$

   where **n** is the molecular director, ε_0 is the dielectric permitibility in the vacuum, $\Delta\varepsilon = \varepsilon_\parallel - \varepsilon_\perp$ is the dielectric anisotropy at optical frequencies. $\varepsilon_\parallel$ and $\varepsilon_\perp$ are the dielectric constant for **E** parallel or perpendicular to **n**, respectively. Since the reorientation scales linearly for low power (Δn also increases linearly), a similarity between Kerr nonlinearity and reorientational nonlinearity is established. For high intensity the LC fully reorient and therefore 'saturates'.

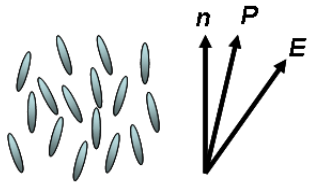

Figure 2.8: .

Notice that for a symmetric molecule $\varepsilon_{\parallel} = \varepsilon_{\perp}$ and $\Delta\varepsilon = 0$ then $\mathbf{P} = \varepsilon_0 (\varepsilon - 1) \mathbf{E}$ describes the relation between polarization and the electric field for isotropic materials.

2. As a result of the induced polarization an optical torque $\vec{\Gamma}_{opt}$ is observed Fig.2.9, and described by Eq.2.12:

$$\vec{\Gamma}_{opt} = \langle \mathbf{P} \times \mathbf{E} \rangle = \varepsilon_0 \Delta\varepsilon (\mathbf{n} \times \mathbf{E}) (\mathbf{n} \cdot \mathbf{E}) \tag{2.12}$$

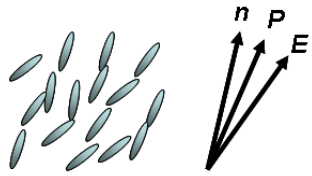

Figure 2.9: .

The bracket denotes the average over the optical cycle.

3. The director rotation is opposed by surface anchoring plus bulk elasticity, and the ensuing torque balance determines the final reorientation of the molecular director **n** achieved at steady-state. The transient dynamics is controlled by the director rotational viscosity.

4. The rotation of the molecular director **n** corresponds to a rotation of birefringence axes, and thus to modifying the "effective refractive index" n_{eff}.

For a rigorous analysis of the interaction between light and liquid crystals, it is necessary to take into consideration the elastic properties of the medium, which

are described by the Frank elastic free energy density K_1, K_2 and K_3 [28]. They are related with the splay, twist and bend elastic constants, respectively. However, by assuming linear restoring torques and considering only one elastic constant described as K, the torque balance equation has the form show in Eq.2.13 [17]:

$$K\frac{d^2\theta}{dz^2} + \frac{\Delta\varepsilon E_0^2}{8\pi}\sin 2(\beta+\theta) = 0, \tag{2.13}$$

where θ is the photoinduced reorientation molecule angle and β is the angle of incidence with respect to the normal to the cell. See Fig. 2.10.

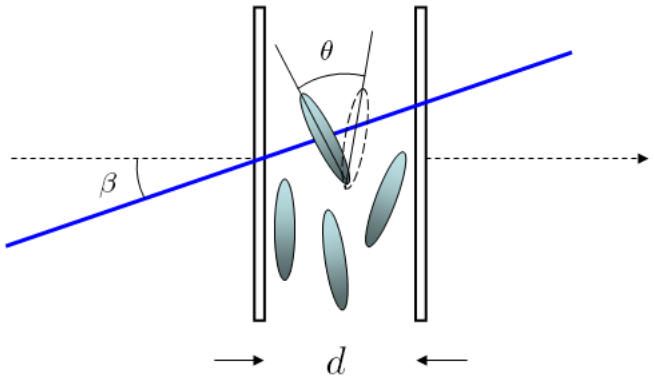

Figure 2.10: Geometry of the illumination upon a liquid crystal cell. β is the angle between the normal to the cell and the illumination, θ is the photoinduced reorientation molecule angle and d is the cell thickness.

In the small θ approximation, Eq. 2.13 may be written as

$$2\xi^2\frac{d^2\theta}{dz^2} + \sin 2\beta = 0, \tag{2.14}$$

where $\xi^2 = 4\pi K/[\Delta\varepsilon E_0^2]$. If the study uses the hardboundary condition, which means that the director axis is not perturbed at the boundary ($\theta = 0$ at $z = 0$ and $z = d$) [29], the solution of Eq. 2.14 is

$$\theta = \frac{1}{4\xi^2}\ \sin 2\beta\ (dz - z^2), \tag{2.15}$$

that is, the reorientation is a maximum at the center and vanishingly small at the boundary of the cell. When averaged over the sample thickness, the factor $(dz - z^2)$ gives $d^2/6$, so that average reorientation angle is

$$\langle\theta\rangle = \frac{\Delta\varepsilon}{16\pi K}\,(\sin 2\beta)\,\frac{d^2}{6}E_0^2. \tag{2.16}$$

As a result of this reorientation, the incident laser suffers a refractive index change $\Delta n(z)$ which, for small θ, is proportional to the reorientational angle as well, $\Delta n(z) \propto \Delta\varepsilon \sin 2\beta\theta(z)$ [17, 29]. By neglecting the z-dependence, it is possible to write the average photo-induced birefringence as,

$$\langle\Delta n\rangle \propto \Delta\varepsilon\,(\sin 2\beta)\,\langle\theta\rangle = n_2 I, \tag{2.17}$$

which is proportional to the light intensity. The nonlinear coefficient n_2 can be written as Eq. 2.18 [17, 29],

$$n_2 \propto \frac{(\Delta\varepsilon)^2}{Kc}\sin^2(2\beta)\,d^2. \tag{2.18}$$

Normally, the average notation is neglected, and the photoinduced birefringence is know as Δn. However, it is assumed that Δn is the average resulting from the integration over the whole cell length.

In addition, from the point of view of the applied torque, reorientation can be induced only when the angle between **n** and **E** is different from zero or $\pi/2$, corresponding to an incidence angle β different from zero. However, it can be demonstrated that, even at normal incidence ($\beta = 0$), reorientation can occur if the input intensity is above a certain threshold. This effect is called the optical Fréedericksz transition, and the threshold intensity, $I_{th} = \pi^2 cK/\Delta\varepsilon d^2$, is given by the balance between the optical and the elastic torques [17, 29].

Even when the nonlinearity of transparent liquid crystals is much large compared with other materials, high intensities focused laser are still needed to achieve these effects. However, it is possible to use photosensitive functional dopants to increase the nonlinearity. These dopants can induce a modification of liquid crystal optical properties. This subject is reviewed in the next section.

2.1.7 Dye-enhancement nonlinear optical properties in azo dye doped liquid crystals

The increase of the nonlinear optical response in a nematic host system due to the presence of a small amount of absorbing azo-dyes, is a phenomenon just discovered in 1990 [24, 30–32]. Actually, Jánossy *et al*. [33] proposed a model in order to explain this enhancement on the nonlinear optical properties of dye doped liquid crystals. By that time, the authors explained this phenomenon as the photoinduced conformational transformations, such as *trans*-*cis* isomerization of dye compounds. They suggested that this transformation can modify the orientational order parameter in absorbing liquid crystals. This phenomenon is known as the *Jánossy effect*.

2.1.7.1 Photoisomerization of azo dyes

Azo dyes are some of the most common used dopants in liquid crystals to obtain colossal nonlinear optical behavior. The name *azo* comes from *azote*, an old name of nitrogen that originates in French and is derived from the Greek *a* (not) + *zoe* (to live). The chemical representation of a general azo dye is shown in Fig.2.11.

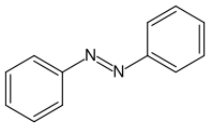

Figure 2.11: Chemical structure of an azo dye.

One of the most interesting properties of azobenzene is the photoisomerization of *trans* and *cis* isomers. Azo dyes are able to absorb strongly light along the dye long axis. Due to this characteristic, the *trans* isomer can be switched to the *cis* one by illuminating with particular wavelengths. In the steady state, the dye molecule has a 'linear-shape' geometry (*trans* isomer), likewise upon illumination, the molecule adopt a 'v-shape' with an angle of 120° (*cis* isomer). The last isomer is less stable than the first one, thus *cis* isomer will thermally or optically relax back to the *trans* via *cis*-to-*trans* isomerization.

Azo dyes are capable to reorient the molecules of materials such as liquid crystals under polarized illumination. Even more, they are also capable to reorient glassy polymers and thin solid molecular films [34]. For this reason, azo dyes are promising materials to be used in nonlinear optics. The photoinduced reorientation in azo dyes can be permanent, and therefore suitable for applications in fields such as optical storage, material optical processing, etc.

In the experiments of this dissertation, 4-dimethylaminoazobenzene-2'-carboxylic acid (methyl red or MR) and 4-dimethylaminoazobenzene (methyl yellow or MY) dyes are used to dope the nematic liquid crystal 4-pentyl-4'-cyano-biphenyl (5CB). In Fig. 2.12 are shown the chemical structure of MY and MR, respectively, as well as the *trans* and *cis* isomers for each dye.

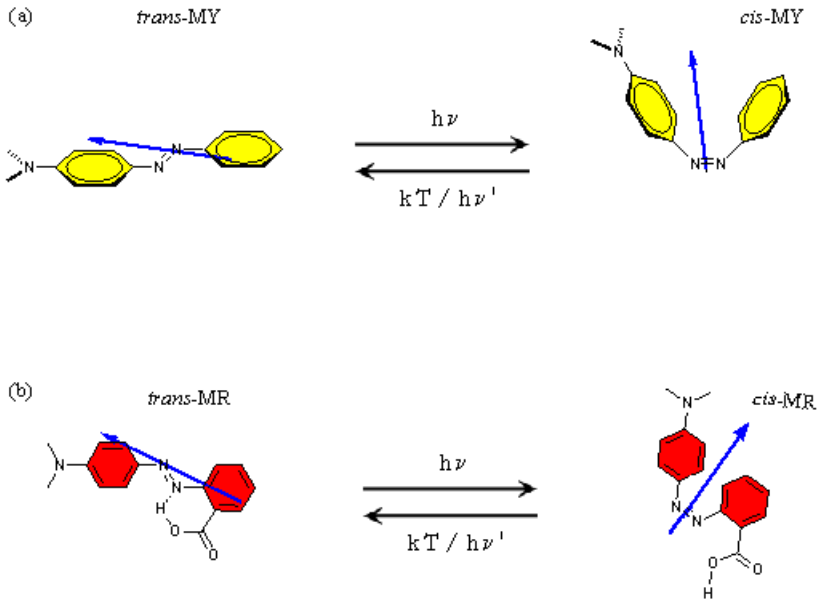

Figure 2.12: *Trans* and *cis* isomers for methyl yellow (a) and methyl red (b). Photo absorption $(h\nu)$ leads to excitation to the *cis* state, whereas thermal relaxation (kT) brings the molecule back to the *trans* state. Arrows show the dipolar momentum orientation for each dye/isomer.

The orientational order in both dye isomers in nematic liquid crystals are different. In fact, *trans* form is significantly more ordered than the *cis* form [35]. Under

these considerations, *trans* and *cis* isomers can be analyzed as two different dopants. Indeed, their different behavior result in an opposite sign in their respective induced optical torque [33]. This means that *trans* and *cis* isomers twist the optical torque in opposite directions.

The *trans-cis* photoisomerization of azo dyes results in drastic changes in the molecular shape, as well as in the distribution of permanent dipole moments in the molecular structure [36]. Thus, in azobenzene-dye doped liquid crystals the photoinduced adsorption of the *cis* isomers on the solid surface leads to the anchoring and alignment of the liquid crystal through dipole-dipole interactions [37, 38]. For this reason, it is very important to mention that the photoisomerization *trans-cis* induce also a change in the dipole moment distribution of the molecules. Actually, the dipole moment change upon photoisomerization for MY and MR are 2.72D and 1.97D, respectively. Furthermore, the dipolar moments in the *cis* conformation for both dyes are very similar (4.46D and 4.56D, respectively) [39]. Therefore, one should expect similar anchoring behavior in both dyes. However, while MR presents permanent anchoring to the confining plates when illuminated, MY presents non anchoring to the substrate.

2.1.7.2 Jánossy effect

By doping a liquid crystal with a minute amount of some dyes, the resulting torque can be enhanced by sometimes more than an order of magnitude. Then, the total torque $\vec{\Gamma}_{tot}$ can be written as the sum of the optical and the dye-enhanced torque:

$$\vec{\Gamma}_{tot} = \vec{\Gamma}_{opt} + \vec{\Gamma}_{dye}, \tag{2.19}$$

where $\vec{\Gamma}_{opt}$ is the optical torque present in transparent liquid crystal due to the presence of the electric field of a laser beam. Likewise, $\vec{\Gamma}_{dye}$ is called the dye-induced torque and can be expressed as the same form as the optical torque in equation 2.12,

$$\vec{\Gamma}_{dye} = \varepsilon_0 \varsigma (\mathbf{n} \times \mathbf{E}) (\mathbf{n} \cdot \mathbf{E}) = \eta \vec{\Gamma}_{opt}. \tag{2.20}$$

The constant ς is dimensionless and depends on dye concentration and molecular structure of both, dye and nematic host. Dye-induced enhancement of the optical torque in nematic LC's can be quantified by the relation between ς and the dielectric anisotropy: $\eta = \varsigma/(n_e^2 - n_o^2)$, known as *enhancement factor*.

In the case of azo dye there is an additional complication due to the conformational change of the molecule. See Section 2.1.7.1. Each isomer (*trans* and *cis*) has different absorption spectra and different orientational order in the nematic. A model to describe the *trans-cis* photoisomerization was developed by Jánossy and Szabados [33, 35].

The mechanism of the *trans-cis* isomerization is illustrated schematically in Fig. 2.13. The configurational coordinate may correspond e.g. to a rotation of one of the central bonds about the double nitrogen bond. Here *trans-cis* transitions involve electronic excitation followed by a relaxation of the nuclear coordinates towards the minimum energy of the excited state. After de-excitation, a further relaxation process takes place, which can lead, with a certain probability, to the stabilization of the *cis* form. In a similar way, light-induced *cis-trans* transitions can also occur.

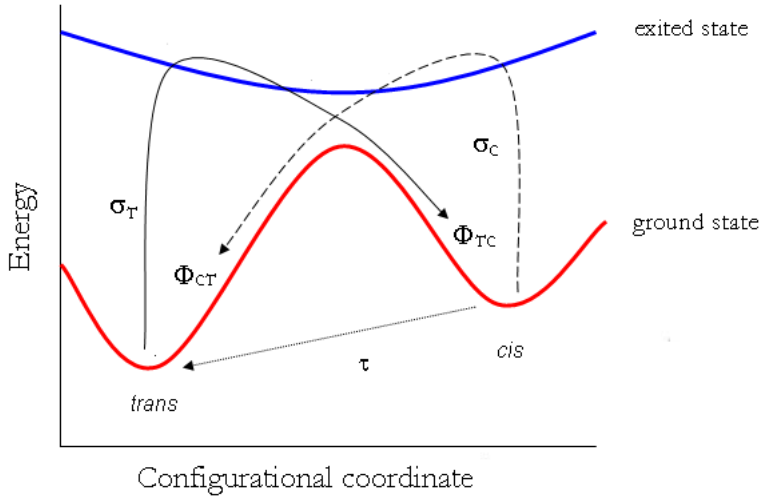

Figure 2.13: Schematic representation of the *trans-cis* isomerization. Solid and dashed lines represent *trans-cis*, *cis-trans* light induced transitions, and straight line represents *cis-trans* thermal transitions.

In Figure2.13 Φ_{TC} and Φ_{CT} are the quantum efficiencies of the *trans-cis* and *cis-trans* transitions, respectively. σ_T^i and σ_C^i are the cross section of absorption of a photon with energy $h\nu$ for a *trans* and a *cis* isomer, respectively, averaged over the orientational distribution function of a relevant isomer. The index i refers to a polarization direction of a pump beam; it can correspond to the extraordinary (e) or ordinary (o) ray (parallel or orthogonal to the long axis molecule). For the extraordinary ray, the averaged cross sections depend on the angle between the wave vector of the light beam and the director, and τ is the relaxation time for *cis-trans* transitions.

Upon illumination, photoisomerization takes place, thus the concentration of *cis* molecules (N_C) is described by the rate equation Eq.2.21:

$$\frac{dN_C}{dt} = (N_T\sigma_T^i\Phi_{TC} - N_C\sigma_C^i\Phi_{CT})I/h\nu - N_C/\tau. \tag{2.21}$$

The first term of Eq. 2.21 describes photo-induced transitions, while the second one represents thermal *cis-trans* transitions. N_T is the concentration of *trans* isomers, I is the light intensity. The third term describes the conversion velocity of *cis* to *trans* isomers.

The microscopic quantities σ_C^i and σ_T^i are connected with the macroscopic absorption coefficients (which can be directly measured) by using the *trans* and *cis* absorption coefficients through the definitions

$$\alpha_T^i = N\sigma_T^i, \quad \alpha_C^i = N\sigma_C^i, \tag{2.22}$$

where $N = N_T + N_C$, is the total number of dye molecules per unit volume. For a system which contains a fraction of cis isomers $(X = N_C/N)$, the attenuation of a weak probe beam, polarized along the m direction, can be described by an absorption coefficient that is a linear superposition of the contributions from the *trans* and *cis* isomers

$$\alpha^m = (1 - X)\alpha_T^m + X\alpha_C^m. \tag{2.23}$$

Under the influence of a pump beam with intensity I and polarized along i, in steady state conditions $(dN_C/dt = 0)$ the equilibrium *cis* fraction, $X = X_{eq}^i$ is

$$X_{eq}^{i} = \frac{X_S^i}{1 + I_S^i/I}. \tag{2.24}$$

In Eq.2.24 X_S^i is the saturated value of *cis* isomers fraction. From the rate equation 2.21, it is possible to relate the saturation values I_S^i and X_S^i,with the parameters of the model as

$$I_S^i = \frac{h\nu}{\tau(\sigma_C^i \Phi_{CT} + \sigma_T^i \Phi_{TC})}, \tag{2.25}$$

and

$$X_S^i = \frac{\sigma_T^i A}{\sigma_C^i + A\sigma_T^i} = \frac{\alpha_T^i A}{\alpha_C^i + A\alpha_T^i} \quad \text{with} \quad A = \Phi_{TC}/\Phi_{CT}. \tag{2.26}$$

Figure 2.14 shows the intensity dependence of the fraction of *cis* isomers for different saturation values X_S and with a specific I_S value.

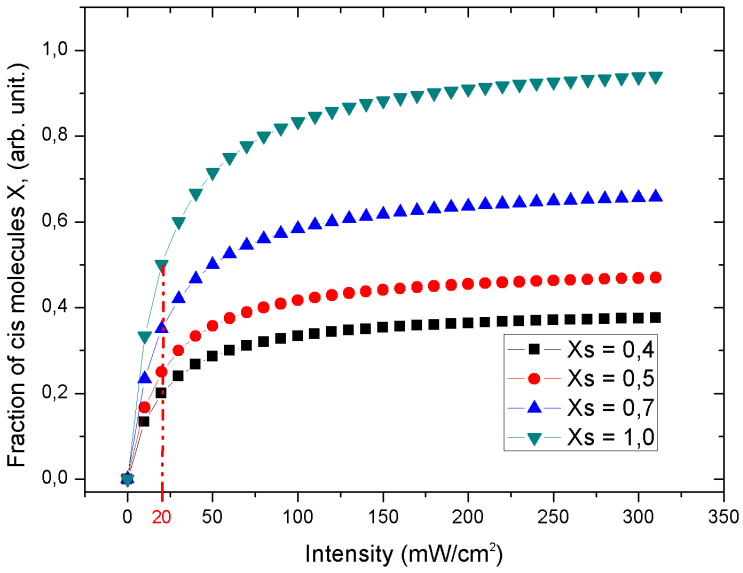

Figure 2.14: Fraction of *cis* molecules as a saturable absorber represented in equation 2.24 for $X_S = 0.4,\ 0.5,\ 0.7,\ 1.0$, and $I_S = 20mW/cm^2$.

The rate equation 2.21 can also be written in function of the probabilities that a *trans* or a *cis* molecule is excited within a unit time. These probabilities are called p_T and p_C, respectively, and the rate equation is defined as

$$\frac{dN_C}{dt} = -N_C(p_C\Phi_{CT}/\tau) + N_T p_T \Phi_{TC}. \tag{2.27}$$

In steady state and knowing that $N_C = NX$ and $N_T = N(1-X)$, the fraction of *cis* molecules X, can be given in function of time as follows

$$X = \frac{X_{sat}}{1+\tau_0/\tau} \tag{2.28}$$

with

$$X_{sat} = \frac{p_T\Phi_{TC}}{p_T\Phi_{TC} + p_C\Phi_{CT}}, \quad 1/\tau_0 = p_T\Phi_{TC} + p_C\Phi_{CT}. \tag{2.29}$$

Here τ_0 is the characteristic time for the formation of the steady state *cis* concentration. It decreases as the light intensity is increased; in the limit $\tau_0/\tau << 1$ the fraction of *cis* isomers approaches the saturation value X_{sat}.

On the other hand, Barnik *et al*. found that the optical torque depends on the light polarization in azo dyes but not in anthraquinone [40]. Janossy and Szabados proposed a model to explain Barnik's results and confirmed their model in azo dye doped liquid crystals. They found that in the low level intensity and low dye concentration limits, the *trans* and *cis* excitation probabilities p_T and p_C are proportional not only to the illumination intensity but also to the angle between the direction of polarization and the director Ψ, [33]. This is natural considering the probability of photon absorption parallel and perpendicular to long axis. To probe that it is necessary first to consider the dissipated energy per unit time and volume in a single dye doped:

$$D = \hbar\omega N p. \tag{2.30}$$

Macroscopically, the dissipation is given by

$$D = \varepsilon_0 \omega \mathbf{e}\, \underline{\varepsilon}''\, \mathbf{e} I, \tag{2.31}$$

where $\underline{\underline{\varepsilon}}''$ is the imaginary part of the dielectric tensor, (Eq.2.6) I is the intensity of the electric field ($I \propto E^2$), and **e** is a unit vector along the electric field. The components of $\underline{\underline{\varepsilon}}''$, as for any tensor in a nematic liquid crystal, can be written as $\varepsilon''_{ij} = \varepsilon''_{\perp}\delta_{ij} + (\varepsilon''_{\parallel} - \varepsilon''_{\perp})n_i n_j$, where **n** is the director, i.e., the symmetry axis of the system [29]. Therefore

$$\mathbf{e}\,\underline{\underline{\varepsilon}}''\mathbf{e} = \varepsilon''_{\perp} + (\varepsilon''_{\parallel} - \varepsilon''_{\perp})\cos^2\Psi, \tag{2.32}$$

where Ψ is the angle between the director **n** and the polarization direction **e**. Comparing Eq.2.30 with Eq.2.31 and replacing Eq.2.32 in this relation, one can find the next expression for the probability

$$p = \left[f_{\perp} + (f_{\parallel} - f_{\perp})\cos^2\Psi\right] I, \tag{2.33}$$

with $f_{\perp} = \varepsilon''_{\perp}/N\hbar$, and $f_{\parallel} = \varepsilon''_{\parallel}/N\hbar$.

Therefore, the probabilities p_C and p_T became

$$p_C = \left[c_{\perp} + (c_{\parallel} - c_{\perp})\cos^2\Psi\right] I, \tag{2.34}$$

$$p_T = \left[t_{\perp} + (t_{\parallel} - t_{\perp})\cos^2\Psi\right] I, \tag{2.35}$$

where $c_{\perp}$, $c_{\parallel}$, $t_{\perp}$ and $t_{\parallel}$ are constants for a particular dye and depend on the orientational order of *trans* and *cis* isomers.

Substituting p_C and p_T in Eq.2.24, the saturation value of the fraction of *cis* isomers dependence on Ψ is found

$$X_S = X_{ord}\frac{1 + g\cos^2\Psi}{1 + h\cos^2\Psi}, \tag{2.36}$$

X_{ord} represents the saturated *cis* concentration for polarization perpendicular to the director and is given by

$$X_{ord} = \frac{At_{\perp}}{At_{\perp} + c_{\perp}}. \tag{2.37}$$

Likewise, g and h are molecular parameters determined by transmission measurements and given by these equations:

$$g = \frac{t_{||} - t_{\perp}}{t_{\perp}}, \tag{2.38}$$

$$h = \frac{A(t_{||} - t_{\perp}) + c_{||} - c_{\perp}}{At_{||} + c_{\perp}}, \tag{2.39}$$

where

$$A = \frac{\Phi_{TC}}{\Phi_{CT}}. \tag{2.40}$$

The transmission measurements needed to find the g and h parameters, and to know the X behavior, are detailed in the following lines. The probe transmission is given by $T = T_0 \exp^{-\alpha_z d}$, where T_0 is the transmission of an undoped sample, d is the sample thickness, α_z gives the attenuation of the probe beam along the z direction (normal to the plates). α_z can be given as a linear superposition of the contributions from the two isomers:

$$\alpha_z = X\alpha_C + (1 - X)\alpha_T. \tag{2.41}$$

The measurements without a pump beam correspond to $X = 0$, while for X_S and X_{ord} a parallel or perpendicular polarized pump to the director, respectively, is required. Denoting the corresponding transmissions by T_T (no pump), T_S (parallel polarized pump), and T_{ord} (perpendicular polarized pump) we have

$$T_T = T_0 \exp^{-\alpha_T d}, \tag{2.42}$$

$$T_S = T_T \exp^{-(\alpha_C - \alpha_T)X_S d}, \tag{2.43}$$

$$T_{ord} = T_T \exp^{-(\alpha_C - \alpha_T)X_{ord} d}. \tag{2.44}$$

From these equations it is possible to obtain

$$X_S / X_{ord} = \frac{\ln T_S/T_T}{\ln T_{ord}/T_T}, \tag{2.45}$$

and therefore it is possible to deduce g and h parameters by fitting them.

As mentioned before, the enhancement factor can be treated as the contribution of two different dyes. One of them due to the *cis* isomers and the other one due to the *trans* isomers fraction. Therefore, the equation for the enhancement factor η can be expressed by

$$\eta = X\eta_C + (1 - X)\eta_T = \eta_T + (\eta_C - \eta_T)X, \tag{2.46}$$

where η_C and η_T are the enhancement factors for the *cis* and *trans* isomers, respectively. It is important to stand out that η_C and η_T have no angular polarization dependence, while X and thus η depend on the angle between the director and polarization direction, Ψ. If the light is high enough to saturate the *cis* concentration ($X = X_S$) the angular dependence of η is

$$\eta = \eta_T + (\eta_C - \eta_T)X_S, \tag{2.47}$$

where X_S is given by Eq.2.36. In Fig.2.15 enhancement factor in function of the angle Ψ is plotted for R4 dye [33].

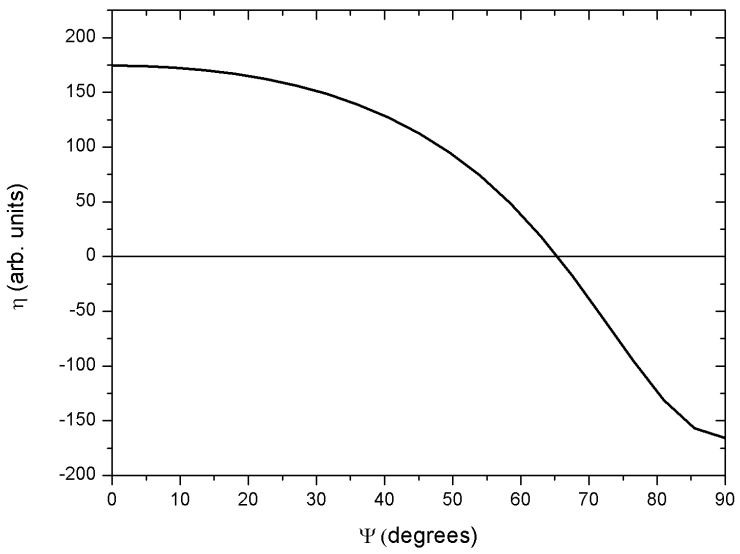

Figure 2.15: Enhancement factor η, dependence on Ψ, where $g = 10.1$, $h = 3.52$, $X_{ord} = 0.26$, $\eta_T = 500$, $\eta_C = -400$ [33].

Briefly, Jánossy *et al*. found that the optical torque produced by *cis* isomer is positive, while for the *trans* isomer is negative. The resultant enhancement factor is reduced due to the competition of both isomers. The polarization dependence will be quite useful in the phase contrast experiments discussed later.

2.1.7.3 Colossal nonlinearity in azo-dye doped liquid crystals

The nonlinear refractive index of the liquid crystals increases many orders of magnitude when doped with azo dyes. This enhancement has been adjudicated to the azo dye photo-isomerization. In 2004, Lucchetti *et. al* [1] reported experimental evidence of the highest value ever published of the nonlinear refractive index coefficient $(n_2 > 10^3 cm^2/W)$ in liquid crystalline materials. They called this nonlinearity *colossal* and it was adjudicated to the anchoring conditions. These *colossal* effect was later reported to be near the nematic to isotropic phase transition temperature, and attributed to the onset of critical opalescence and pretransitional effects [10].

2.1.8 Nonlinear optical measurements of dye-doped nematic liquid crystals

Several techniques are used to characterize the nonlinear optical behavior of dye-doped liquid crystal cells. One of them consists in the holographic grating diffraction formation. An Argon laser is employed to induce the nonlinearity and a weak He-Ne laser is used to probe and measure this behavior.

Other common method to characterize nonlinear materials is know as Z-scan. In this technique the monitoring of the transmittance variations of samples as function of the sample position is scanned around the focal point of a fast lens. In both methods it is possible to measure the nonlinear optical response not only in function of intensity but also in function of its polarization direction.

In this dissertation the first technique was used to characterize the nonlinear coefficient in function of intensity and polarization in the samples and the results obtained in these experiments are reported in chapter 3. In addition, some Z-scan measurements in Ref. [14] are used to complement the information. Next section presents a brief review of both techniques.

2.1.8.1 Grating diffraction formation

The holographic grating formation consists in illuminating a liquid crystal cell with an interference pattern produced by two pump beams with total intensity I_p and wavelength λ. Due to the local refractive index change, the light intensity distribution in the interference pattern creates a phase grating inside the cell i.e., in the bright fringes the molecules are reoriented due to the presence of the electric field, while in dark fringes there is no reorientation (Fig.2.16). In order to probe the diffraction efficiency ζ of the grating, a probe beam illuminates the cell.

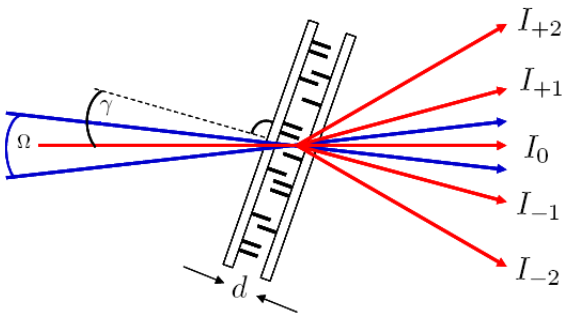

Figure 2.16: Scheme of a holographic grating in the LC sample due to an interference pattern of two coherent Ar^+-laser beams (blue) which cause a refractive index modulation. A He Ne-laser (red) beam impinging the sample results in diffracted beams of zero-, first- and second-order. d is the thickness of the sample, γ the angle between the incident He Ne-laser beam and Ω the interference angle of the Ar^+-beams.

The diffraction efficiency ζ is defined as the ratio between intensity I_{+1} of the first order of diffraction and the total probe beam intensity I_0, that is [22]:

$$\zeta = \frac{I_{+1}}{I_0}. \tag{2.48}$$

The typical liquid crystal samples thickness d is $5 \rightarrow 20\mu m$. For such reason, in our case we are exclusively working with Raman-Nath gratings valid for $d << \Lambda^2/\lambda$ [20] and therefore we observe several orders of diffraction. Here d is the thickness of the cell, λ is the wavelength of the pump laser, and Λ is period of the grating.

The phase grating can be specified by Λ, the fringe spacing in the interference pattern [41] and defined by

$$\Lambda = \frac{\lambda}{2n\sin(\Omega/2)} \approx \frac{\lambda}{n\Omega} \tag{2.49}$$

where Ω is the wave-mixing angle and n the refractive index of the material.

In the Raman-Nath regime, the first order diffraction efficiency can be calculated as:

$$\zeta = |J_1(\delta)|^2, \tag{2.50}$$

where J_1 is the Bessel function of the first order and the argument $\delta = \Delta n d 2\pi/\lambda$. For $\delta < 1$, the diffraction efficiency can be approximated as

$$\zeta \approx (\frac{\pi \Delta n d}{\lambda})^2, \tag{2.51}$$

and cannot exceed the maximum theoretical value of 34% [42] (See Fig. 2.17).

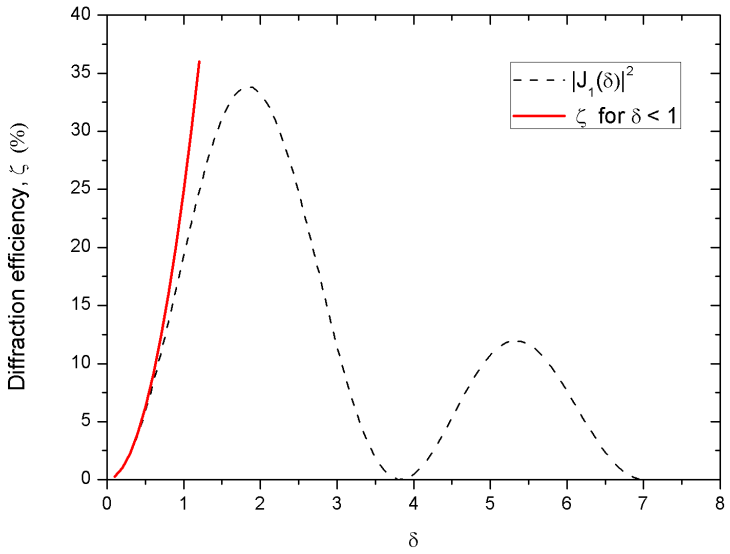

Figure 2.17: Diffraction efficiency at the Raman-Nath regime in Eq. 2.50(dashed line) and the approximation for $\delta = \Delta n d 2\pi/\lambda$ small (solid line).

By replacing $\Delta n = n_2 I_p$ Eq.2.17 into Eq. 2.51, one can find

$$n_2 = \frac{\lambda \zeta^{1/2}}{\pi d I_p}. \tag{2.52}$$

2.1.8.2 Z-scan measurements

The Z-scan is a simple and popular experimental technique to measure intensity dependent nonlinear susceptibilities of materials. In this method, the transmittance of the sample through an aperture is monitored in the far field as a function of position, Z, of the nonlinear sample in the vicinity of the linear optics focal position. The required scan range in an experiment depends on the beam parameters and on the sample thickness d. A critical parameter is the diffraction lenght, Z_0, of the focused beam defined as $\pi w_0^2/\lambda$ for a Gaussian beam, where w_0 is the focal spot size [43].

By varying the aperture in front of the detector, one makes the Z-scan transmittance more or less sensitive to either the real or imaginary parts of the nonlinear response of the material, i.e., nonlinear refractive index and nonlinear absorption, respectively.

A typical Z-scan measurement for a thin sample exhibiting nonlinear refraction, is shown in Fig. 2.18. The solid line in this figure corresponds to a self-focusing nonlinearity, where $\Delta n > 0$. The measurement results in a valley followed by a peak in the normalized transmittance as the sample is moved towards the detector (increasing Z). The positive lensing induced upon the sample results in a greater far field divergence and a reduced aperture transmittance. On the other hand, with the sample placed after focus, the same positive lensing reduces the far field divergence allowing for a larger aperture transmittance. The opposite occurs for a self-defocussing nonlinearity, $\Delta n < 0$ (Fig.2.18, dashed line).

Rodriguez *et al*. [14] reported the characterization of a dye doped liquid crystal sample of methyl red in 5CB using the Z-scan technique with CW illumination at $633nm$. Using a planar cell, they observed the strong nonlinear optical response, both negative and positive. In fact, their measurements show that the sign in the nonlinearity is dependent on the angle between polarization and the director of the LC molecules. Figure 2.19 shows these measurements for an incident power of $4mW$ and different input polarizations.

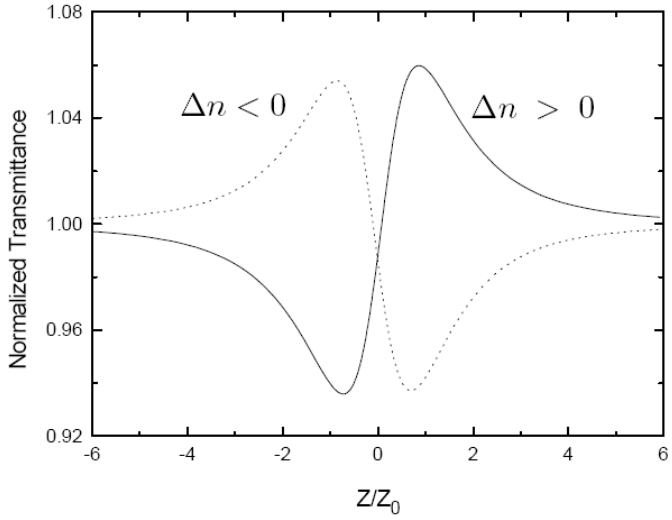

Figure 2.18: A typical Z-scan for positive (solid line) and negative (dashed line) third-order nonlinear refraction at Ref.[43].

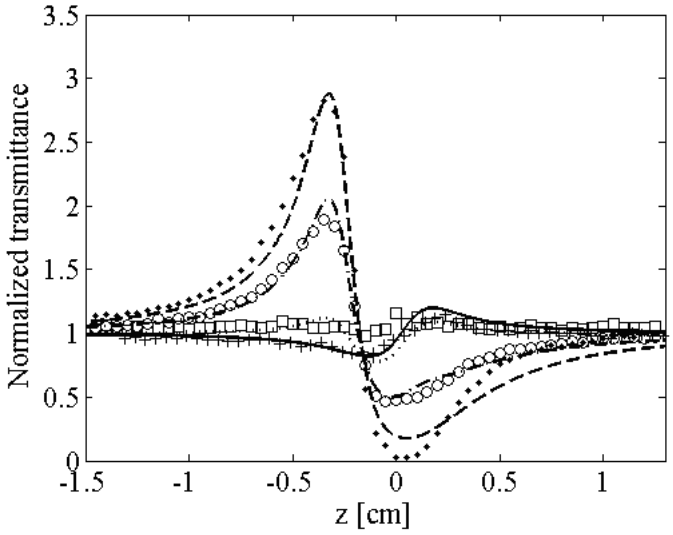

Figure 2.19: Z-scan curves at $633nm$ for incident polarizations of: $0°$(♦), $30°$(○), $60°$(□) and $90°$(+). A $3.5cm$ lens and unexpanded beam ($0.8mm$ diameter) from a He-Ne laser ($\lambda = 633nm$) were used. Sample thickness $20\mu m$ and incident power of $4mW$. Lines are numerical simulations for the same input polarizations. Taken from Ref.[14].

2.2 Phase Contrast Microscopy

Imaging and visualization of phase objects is an outstanding topic in microscopy. In fact, different techniques have been developed to measure and analyze qualitatively and/or quantitatively optical phase disturbances. Among these techniques is the well-known Zernike phase-contrast method, which is able to extract the phase information of small distortions. The phase contrast technique was originally proposed by Frits Zernike in 1934 [44, 45]. This technique employs an optical mechanism to translate minute variations in phase into corresponding changes in amplitude, which can be visualized as differences in image contrast. One of the major advantages of phase contrast microscopy is that living cells can be examined in their natural state without previously being killed, fixed, and stained. As a result, the dynamics of ongoing biological processes can be observed and recorded in high contrast with sharp clarity of minute specimen detail.

Unfortunately, this phase contrast technique presents some problems i.e., difficult alignment, strict fabrication filter requirements, very expensive equipment, among others. However, some of these difficulties can be solved using nonlinear materials. The colossal nonlinearity of dye doped nematic liquid crystal ($n_2 = 100\, cm^2/W$) [1] makes of this material a promising candidate to be used as a Zernike filter, since low power lasers ($\sim 1mW$) are used.

In this section the original phase contrast system proposed by Zernike will be reviewed and a more strict and general mathematical analysis is also included. In addition, the implementation of a phase contrast microscope using a DDLC cell as a nonlinear filter is examined and the advantages exhibited by this material are analyzed.

2.2.1 Classical Zernike Phase-Contrast Microscope

For this mathematical analysis one can consider that the transmittance of a phase object, $f(x, y)$, with small phase variations, $\varphi(x, y) \leq 0.1\pi\ rad$, is coherently illuminated in a common image-forming system. x and y are the spatial coordinates

in the plane perpendicular to the optical axis. By considering the first two terms of the Taylor expansion it is possible to approximate $f(x,y)$ as follows [46]:

$$f(x,y) = \exp[i\varphi(x,y)] \approx 1 + i\varphi(x,y). \tag{2.53}$$

The intensity produced by this phase object is given by

$$I(x,y) \approx |1 + i\varphi(x,y)|^2 \approx 1. \tag{2.54}$$

Nevertheless, in Eq. 2.54 the phase information is not observed because the constant term 1 and $\varphi(x,y)$ are separated by $90°$ in the complex plane, in other words, they are in quadrature. Zernike realized that placing a phase filter in the Fourier plane it is possible to break this quadrature (see Fig.2.20) and thus, visualize phase changes as intensity changes in the image plane. Zernike used a phase filter of $\pm\pi/2$ to perturb the zero order, therefore, the intensity distribution becomes [46]:

$$I(x,y) \approx |\exp(\pm i\pi/2) + i\varphi(x,y)|^2 \approx 1 \pm 2\varphi(x,y). \tag{2.55}$$

In Eq. 2.55 a linear relation between phase changes and intensity distribution is obtained i.e. phase changes can easily be quantified taken into consideration the contrast of the images. For $1+2\varphi(x,y)$ the contrast in the images is referred as *positive phase contrast*, while for $1-2\varphi(x,y)$ is referred to as *negative phase contrast*. It means a phase retardation of $+\pi/2$ or $-\pi/2$, respectively.

A schematic representation of the system is shown in figure 2.20.

The object wave is divided into the undiffracted and diffracted light. The undiffracted wave (zero order) is perturbed in phase by the Zernike filter. In the observation plane, the diffracted and undiffracted waves interfere producing an intensity distribution where the phase object is visualized. In order to achieve this shift phase in the undiffracted light, only a small circular phase plate is placed in the Fourier plane. Therefore, the radius of the phase filter is typically smaller than the diffraction limited radius of a undistorted focused input wave [47].

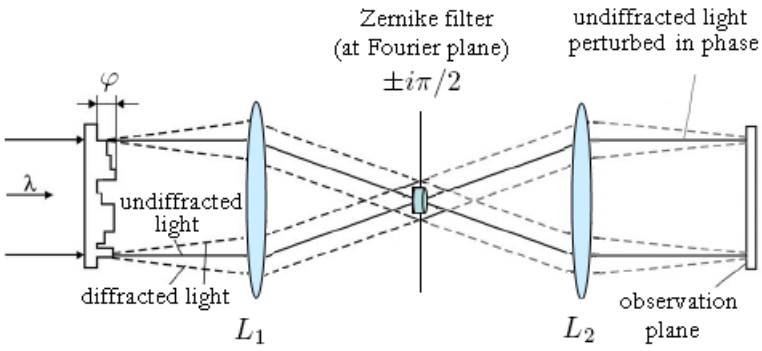

Figure 2.20: Implementing phase contrast using a $4f$ system. L_1 and L_2 are the lenses of the system.

2.2.1.1 Fill factor considerations

In order to obtain the highest image contrast, another consideration must be done. It has been proved the necessity to illuminate the object over a considerable area given by the *fill factor*, in order to obtain high contrasted images. This factor is given by equation [48, 49]:

$$\varrho = \frac{Object\ area}{Total\ illuminated\ area}. \tag{2.56}$$

It means that the largest the total illuminated area respect to the object area, the higher the energy of the zero spatial frequency of the Fourier transform. For nonlinear phase contrast it has interesting implications, i.e., the modulation of the nonlinear refractive index.

2.2.2 Nonlinear phase contrast

In phase contrast microscopy, it is desirable that the phase filter alters only the phase in the zero frequency of the Fourier transform (the undiffracted wave). With this purpose a binary phase filter is employed in Zernike phase contrast technique. Unfortunately, the fabrication of the filter requires very high precision and, once constructed, the filter must be placed at the zero frequency of the Fourier plane, which represents a hard task to achieve. Other complications are regarded with the Zernike

filter size: the Fourier transform depends on the object dimensions, that represents an important difficulty to be solved.

However, it is possible to take advantage of nonlinear materials, where a refractive index change can be optically induced. Supposing that a phase object Fourier transform has its maximum intensity at the zero frequency and one would wish to obtain its phase contrasted image. Then, if this intensity distribution addresses a Kerr-type nonlinear material, an apodized Zernike filter is self-induced and the transmitted field generates a contrasted image at the image plane. The high frequencies components of the Fourier Spectrum induce only a low change in the refractive index. Therefore, the Zernike phase change is reached.

It is possible to describe analytically the response of the image forming system taking into consideration the nonlinear material contribution used as a Zernike filter. This analysis also considers the fill factor illumination. The input plane field distribution in one dimension can be represented by next equation [47]

$$f(x) = rect(x) + [\exp\varphi(x) - 1]rect\left(\frac{x}{\varrho}\right), \tag{2.57}$$

where $\varphi(x)$ is the phase object distribution to be visualized and ϱ is the fill factor, which take values between 0 and 1. In this analysis the magnification of the imaging system is assumed to be one. The first term in Eq. 2.57 describes the normalized illuminated area. On the geometrical focal plane of the lens the field distribution is proportional to $F(\nu)$

$$F(\nu) = (1-\varrho)Sinc\left[\frac{1-\varrho}{2}\nu\right]\cos\left[\frac{\pi}{2}\nu(1+\varrho)\right] + \varrho Sinc(\varrho\nu) \otimes \mathcal{F}\left\{\exp(\varphi(x))\right\}, \tag{2.58}$$

where $\otimes$ represents convolution, $Sinc(x)$ is equal to $[\sin(\pi x)]/\pi x$ and $\mathcal{F}$ denotes the Fourier transform operator. When the fill factor is small ($\varrho \leq 0.1$), the first term of Eq. 2.59 dominates the Fourier plane intensity distribution. In this case, if the nonlinear medium photoinduced phase change is proportional to the intensity across all the dynamic range, a relative narrow phase filter is induced that resembles a Zernike-type filter. However, the photoinduced phase is no constant around the zero frequency area. It decreases rapidly from a maximum value at the zero frequency to a minimum

(zero) at the frequency $\nu = \pm(1+\varrho)^{-1}$. Under these circumstances and considering an intensity dependent nonlinearity response proportional to the intensity, or Kerr-type nonlinearity, the photoinduced filter may be approximated by

$$H(\nu) \approx 1 + rect\left[\frac{\nu}{2}(1+\varrho)\right]\left[\exp(i\alpha|c(\nu)|^2) - 1\right], \tag{2.59}$$

where α is a constant determined by the nonlinear medium properties and $c(\nu)$ represents the first term of Eq.2.58. The photoinduced filter transmittance of $H(\nu)$ has been approximated to one outside of the main lobe width.

The resulting field distribution on the image plane can be given by $\mathcal{F}^{-1}\{F(\nu)\cdot H(\nu)\}$ and is proportional to the image of the object $f(x')$ added to a fill factor, which describes the phase object visualization

$$i(x') \approx f(x') + \frac{2}{1+\varrho} Sinc\left[\frac{2x'}{1+\varrho}\right] \otimes \mathcal{F}\left\{\exp(i\alpha|c(\nu)|^2) - 1\right\} \otimes \left[rect(x') - rect\left(\frac{x'}{\varrho}\right)\right]. \tag{2.60}$$

This is a general expression to describe nonlinear phase contrast, however, since the analysis is not an easy task, a numerical analysis is required.

2.2.3 Phase contrast of a $\pi/2$ binary phase object

By using linear phase filtering, the phase contrast can be calculated for a binary phase object $f(x)$ given in expression 2.57 with a phase change of $\varphi = \pi/2$,

$$f(x) = rect\left(\frac{x}{T}\right) + [\exp(\pi/2) - 1] rect\left(\frac{x}{t}\right), \tag{2.61}$$

where T is the total illuminated area and t is the object area.

If the fill factor is 0.1 and the phase in the filter is $\pi/2$, the intensity distribution is ploted in Fig. 2.21:

In order to evaluate the performance of the phase contrast system, the image contrast can be computed as $C = (I_{\varphi_{max}} - I_{\varphi_{min}})/(I_{\varphi_{max}} + I_{\varphi_{min}})$, where $I_{\varphi_{max}}$ and $I_{\varphi_{min}}$ correspond to the field distribution intensities for the maximum and minimum phase change in the object. For this particular case, $\Delta\varphi = \pi/2$ and the contrast in the images as function of the phase in the filter is shown in plot 2.22

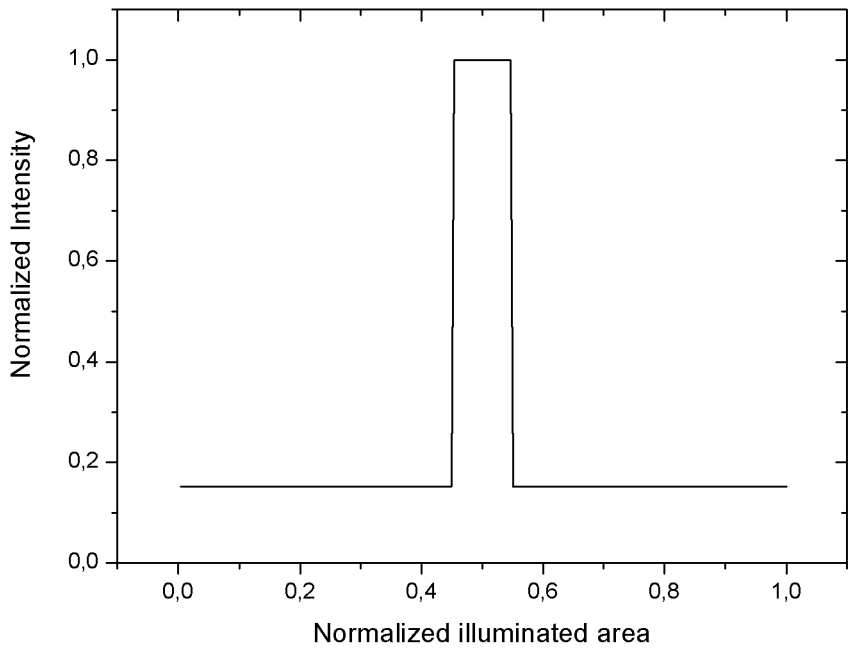

Figure 2.21: Contrasted intensity distribution for $\varphi = \pi/2$, $\rho = t/T = 0.1$ and $\theta = \pi/2$.

As mentioned before, the behavior of dye-doped liquid crystals when used as a Zernike filter gives many advantages. The colossal nonlinear optical behavior allows the use of weak lasers to induce the change on the refractive index to achieve the Zernike filter. Likewise, the fraction of *cis* isomers dependence on the light polarization direction suggest the possible to adjust the optical torque induced by the dye in the LC sample, hence, tune the image contrast. However, it is worth to mention that the number of *cis* isomers upon illumination reach a saturation level given by (X_S) in expression 2.24 $(X = \frac{X_S}{1+I_S/I})$. This equation also predict the range of linear dependence between the fraction of *cis* isomers and intensity.

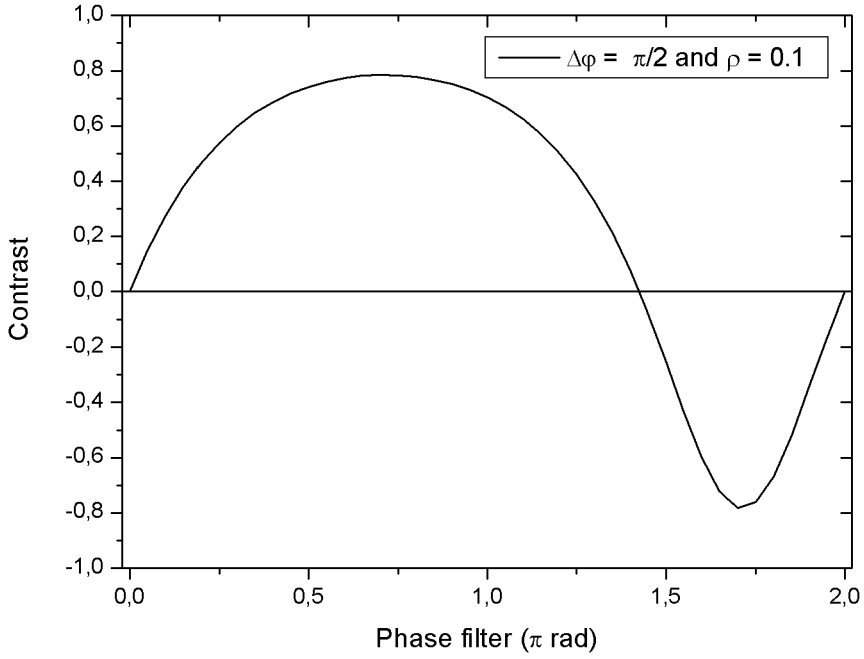

Figure 2.22: Contrast for phase filters values between 0 and 2π

Chapter 3

Characterization of the Nonlinear Optical Properties of Azo Dye-Doped Liquid Crystals

3.1 Introduction

The enhancement of the molecular reorientation in dye doped liquid crystals (DDLC) have been deeply investigated for the last decades due to their colossal optical non-linearity which leads to attractive low power applications. The origin of the enhancement of the nonlinear optical properties is attributed to the dye molecular reversible photo-transformation. This phenomenon presents an outstanding refractive index dependence on polarization and intensity illumination. However, it also presents some side-effects not completely understood i.e., permanent dye anchoring to the substrate, among others. The understanding and characterization of the phase change induced by a polarized beam and its effects are relevant for the applications related with this research work.

The objective of this chapter is to report the experiments performed in DDLC in order to clarify the photoinduced molecular mechanisms present in an azo DDLC sample when illuminated by a linearly polarized laser beam.

This chapter includes: i) the study of the permanent diffraction gratings in azo dye doped liquid crystal cells, ii) the anisotropic behavior of these gratings as function of the probe beam, iii) the response and relaxation time and iv) its saturable absorber response as function of the polarization and intensity pump beam, v) the g and h parameters of a 5CB-MR1% doped planar cell (found by transmission measurements detailed in section 2.1.7.2). Finally, a discussion of the information obtained with these results is presented.

3.2 Azo-dye-Induced Effects on Permanent Grating Recording

It is known that the azo-dye molecules photoisomerization is responsible for the increase of many orders of magnitude of the nonlinear refractive index of DDLCs [1,27,33,50]. It has been also suggested that the substrate plays an important role in the LC nonlinear optical behavior [1,37]. In fact, Komitov *et. al.* [37,38] suggested that dye anchoring lead to alignment of bulk liquid crystal through dipole-dipole interactions. Photoinduced adsorption of the dye on the substrate produces permanent gratings which may be undesirable side effects in dynamic holography and other applications [39]. On the other hand, permanent gratings may be useful in optical memories or in optical routers, etc [11]. Therefore, the understanding of the molecular mechanisms involved in dye anchoring is crucial in order to control it or even to eliminate dye anchoring.

The study presented here, comprises the performance comparison of two azo dyes: Methyl red (MR) and methyl yellow (MY) azo dyes (Aldrich). The main difference between these dyes is the acid group presence positioned in the phenyl ring i.e. $2' - COOH$ on MR (See Fig.3.1) [51]. This leads to a difference in the absorption spectra of both organic compounds (Fig.3.2) The absorption spectra are similar, except that for MY the peak absorption is blue shifted ($\sim 400nm$) while for MR is around $500nm$. Both dyes were dissolved in the nematic host at concentration per weight of 1.0% and nematic liquid crystal 5CB (Merck) was used as the host liquid crystal material. The first dye presents permanent grating formation, while the second one does not.

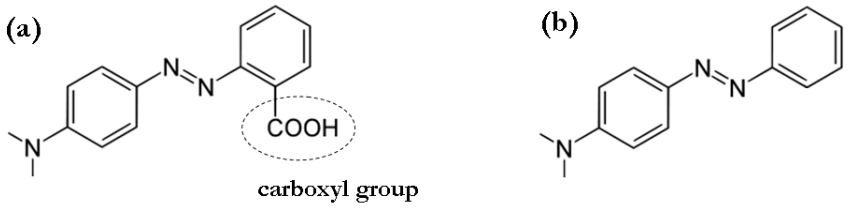

Figure 3.1: Chemical structure of (a) MR and (b) MY. The carboxyl group (-COOH) is the polar group in the MR molecule [39].

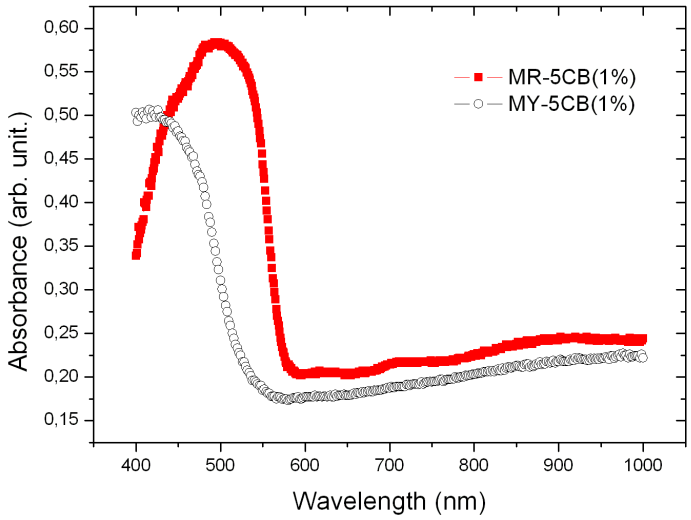

Figure 3.2: Absorption spectrum of MR and MY in 5CB liquid crystal at 1.0% wt.

The glass substrates were cleaned thoroughly using a piranha solution as a common promoter to increase the $-OH$ group population on the glass surface substrates [52], and thus, enhance their hydrophilic properties. Although permanent gratings can be recorded under different surface treatments (surfactants, rubbing films (PVA), and ITO alone) it is well known that piranha solution enhance the superficial density of $-OH$ groups. A sandwich glass cell $(d \approx 3 - 5\mu m)$ filled with the host-guest mixture was used in the experiments. The sample is randomly oriented since no treatment layers were used.

3.2.1 Experimental results

The experimental setup consists of a pump-probe scheme as shown in Fig.3.3. The pump is provided by an Ar^{+} ion laser ($\lambda = 514.5nm$ at $\sim 34mW/cm^2$) which was used to record $20\mu m$ gratings period. The pump wavelength is nearly the maximum value in the absorption spectra of the MR (Fig.3.2), so that the MR photoisomerization of the dye is facilitated. A weak He-Ne laser ($\lambda = 633nm$) was used to measure the diffraction efficiency of the grating (See section 2.1.8.1). The probe's beam polarization is parallel to the pump beam. The spot size of the probe beam is approximately 6 times smaller than the recording one. The received signal from the photodetector was processed by a lock-in-amplifier and the data were measured and saved with a LabView program and a computer.

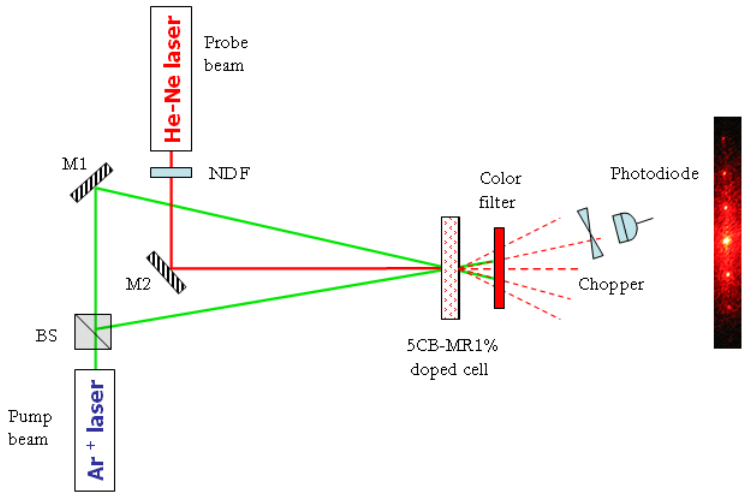

Figure 3.3: Schematic experimental set-up.

As can be observed in Fig.3.4, permanent diffraction gratings can not be obtained for MY doped samples, curve (a). Before grating recording, the intensity level of the probe beam shows a stable value. Once the pump beam is on, the diffraction grating starts to forme, hence, the diffraction efficiency increases. After $\sim 150sec$ upon illumination, the diffraction grating reaches its maximum value ($\sim 0.27\%$). Nevertheless, when the pump laser is turned off, the probe beam value decays to its original value

after $\sim 200sec$. That means that there is no permanent grating recorded in the sample. Likewise, diffraction gratings were recorded in the MR doped sample. The stationary value of the diffraction efficiency in a MR cell commonly reaches 0.4% around $100sec$ upon illumination. However, in this experiment the sample was pumped just for $20sec$ to demonstrate that even with this short exposure time the permanent grating can be recorded, as shown in Fig.3.4.

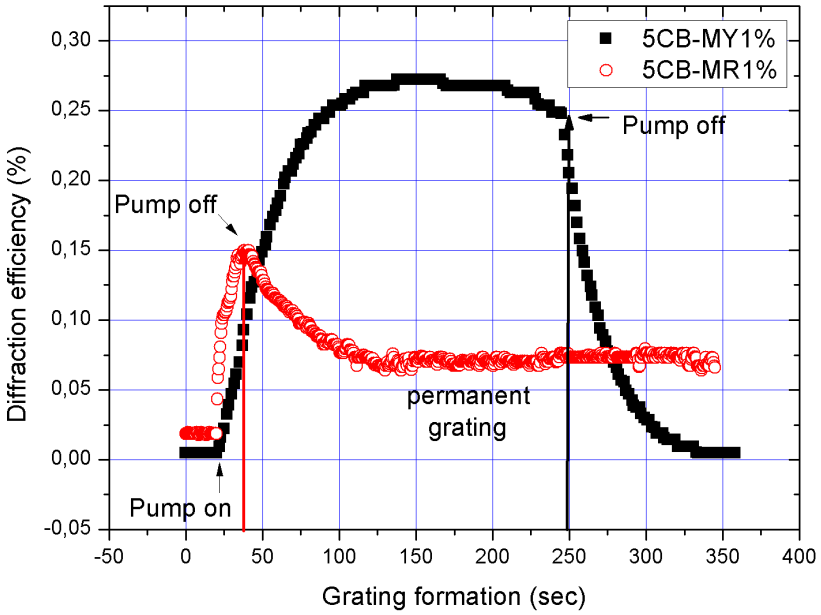

Figure 3.4: Permanent and transient grating formation in 5CB doped with methyl red (■) and methyl yellow (○), respectively.

This phenomenon has been adjudicated to the molecular anchoring of the MR dye on the substrate [1]. It has been demonstrated that the dipole moment of the *cis* isomers become higher than those for the *trans* isomers, leading to a preferential *cis* structure adsorption on the solid substrate [37, 38]. However, as mentioned before in Section2.1.7.1, the dipole moment change upon photoisomerization has been reported to be for MR and MY, $1.97D$ and $2.72D$, respectively. The dipolar moments in the *cis* conformational for both dyes are very similar ($4.56D$ for MR and $4.46D$ for MY). Based on this information, *cis*-MY species should give rise to a stronger dipole-

dipole interaction, and therefore, stronger permanent gratings formation than *cis*-MR species. This contradiction suggests the presence of other mechanisms which must be taken into consideration.

Since MY does not exhibit permanent gratings, the grating is attributed only to the dye-induced reorientation of the liquid crystal molecules in the bulk cell. On the other hand, for MR it is possible to observe that besides of the process present in the MY case, the MR anchoring has an important contribution to the diffraction efficiency.

In order to measure the adsorbed dye contribution of these processes, some samples with the same thickness and dye concentration were prepared containing MR dissolved on liquid crystal (5CB/MR$(99.0 : 1.0\%)$) and on isoprophyl alcohol and dimethylformamide (iPrOH/DMF/MR $(49.5 : 49.5 : 1.0\%)$) solutions (these solvents are not oriented by the dye). The experimental results obtained during the holographic grating formation on these samples are plotted in Fig.3.5.

The diffraction efficiency for the DDLC reaches 0.6% while the dye doped solvent reaches only 0.0037%, i.e. more than two orders of magnitude. Both compounds follow almost the same dynamic but solvents saturates faster, probably due to the lower viscosity (the dyes moves faster towards the substrate). In other words, the contribution of the dye anchoring to the diffraction efficiency is quite small although its effect on the bulk is quite remarkable, indicating that the LC molecules adjoining to the anchored dyes are oriented forming a permanent grating as well. In this point it is worth mentioning that the gratings recorded in both cells are still recorded after 2 years. Figure3.6 shows the grating in iPrOH/DMF/MR1% after evaporation of the solvents. This image was obtained by using the microscope Leica DFC with an objective of 40X.

This fact emphasizes the strong effect on the volumetric reorientation due to the anchoring conditions controlled by the adsorbed dye. After repetitive heating of the sample (about $40°C$) above the clearing point temperature ($32°C$ for 1% wt MR doping) the grating can be erased. It indicates that the anchoring energy is $E_{anc} \sim (0.0263 - 0.0271) joules$.

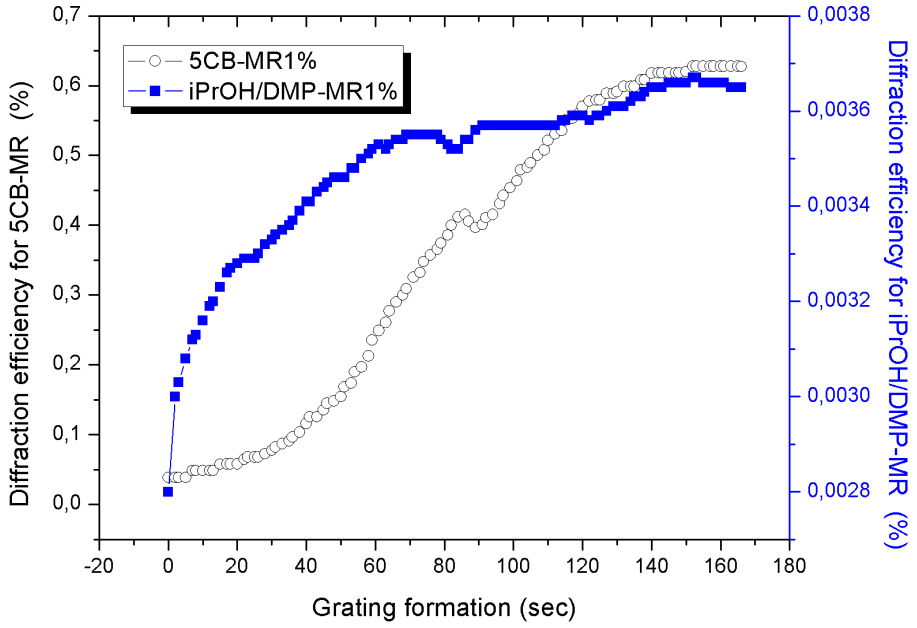

Figure 3.5: Grating diffraction efficiency due to: (○) Adsorbed dye to the substrate and dye induced liquid crystal reorientation, 5CB-MR1% cell (scale on the left). (■) Adsorbed dye, iPrOH/DMF/MR 1% cell (scale on the right).

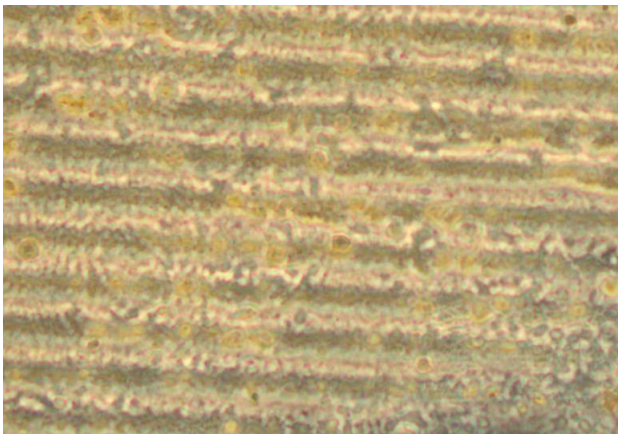

Figure 3.6: Image of the recorded grating in the iPrOH/DMF/MR1% sample. It shows the anchored dye remaning after evaporation of the liquids. The grating period is $\sim 20\mu m$.

3.2.2 Discussion

A first approach to explain the apparent contradiction in the presence of permanent gratings in MR or MY, is to address the strong interaction between the polar group on MR (carboxyl, -COOH) and the hydrophilic surface through intermolecular forces (hydrogen bond, van der Waals, dipole interactions, etc.). Besides, it is well known that the LC orientation has strong dependence on the substrate properties [53, 54]. In addition, polar groups, such as -COOH, -OH and -NH are associated with hydrogen bond interactions [55, 56]. Therefore, it is wise to assume that the molecules with polar nature i.e., carboxyl acid group, have a strong interaction with the terminal -SiOH moieties of the superficial glass substrate [57]. This hydrogen bonding interaction could lead to much better perform in rendering permanent grating formation.

In addition, the *cis*-form has higher polarity than the *trans* counterpart, therefore, they are more strongly attracted by the hydrophilic surfaces through dipolar interactions [39]. Thus, the photoadsorption produces, by its light-induced reorientation, a nematic local order in the bulk of NLC. The direction of the dipole moments are represented in Fig.3.7. Figure3.7(a) shows the dipolar interactions present in *cis*-MY, while, Fig.3.7(b) represents the two-step strong adsorption of the MR on the surface. The first step is caused by an H-bonding of the O-H$\cdots$=C type between -COOH and -OH species on the interface, this interaction is stronger than dipolar factor solely. Upon illumination, the second step takes place: MR molecule quickly attain *cis*-isomer that generates a second hydrogen bond, as shown on right in Fig.3.7(b). In consequence, the MR molecules are strongly anchored to the hydrophilic surface by O-H$\cdots$O=C and O-H$\cdots$O double hydrogen bonding. *Trans* is also adsorbed to the substrate but the anchoring energy is smaller than the thermal energy and therefore the bond is easily broken but not in the case of *cis* isomer. The *cis*-phototransformed entity are believed to be oriented approximately perpendicular to the surface of substrate, later we will show that it is not the case.

In Ref. [39] the comparison between permanent and the reorientation grating in a 5CB sample doped with MR is reported. The experiment consists in modulating the

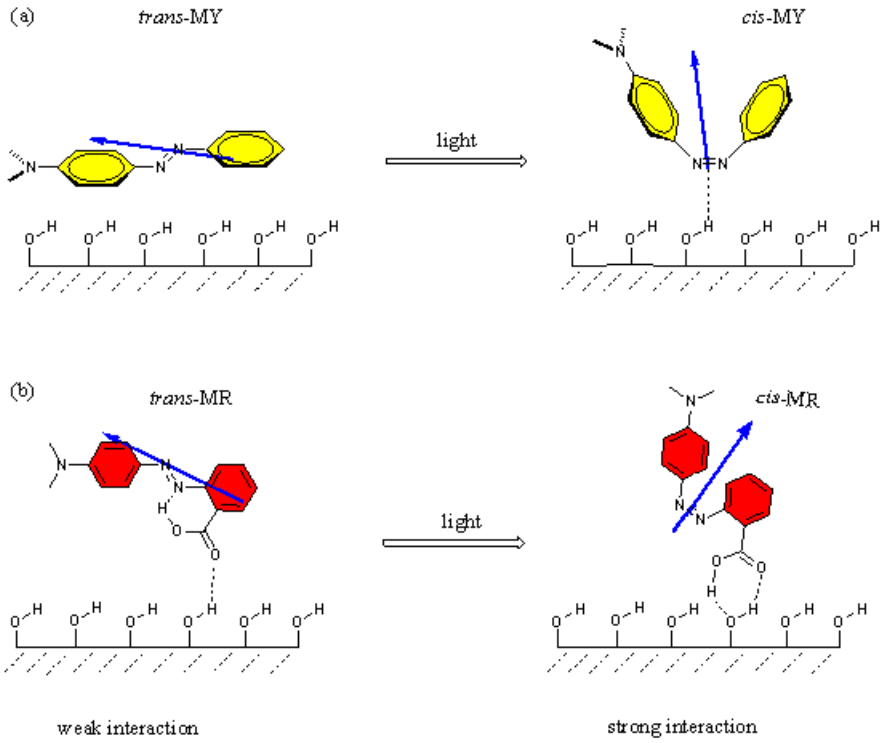

Figure 3.7: Different intermolecular interaction fashions for MY and MR. (a) between the surface and trans-cis-MY species only dipole interactions dominate. (b) Formation of hydrogen bonding on hydrophilic surface by MR molecules: left, trans-MR leads to single hydrogen bonding (weak interaction); right, double hydrogen bonding favored by cis-MR under photo-isomerization (strong interaction).

pump beam (on-off) while the diffraction efficiency was measured. These results are shown in Fig.3.8. One can distinguish the contribution of the permanent grating when the pump is off. As mentioned before, this grating possess two contributions: one due to the adsorbed dye and another one due to the adsorbed dye-induced reorientation of the adjoining LC molecules. The resulting permanent grating leads to reorientation on the bulk liquid crystal represented in Fig.3.8 when the pump is on. This means that the diffraction efficiency measured in 5CB-MR doped is due to presence of three process: *(i)* Bulk dye-induced reorientation of the LC, *(ii)* The adsorbed dye anchored in the substrate and *(iii)* LC molecules reoriented by this thin dye layer anchored.

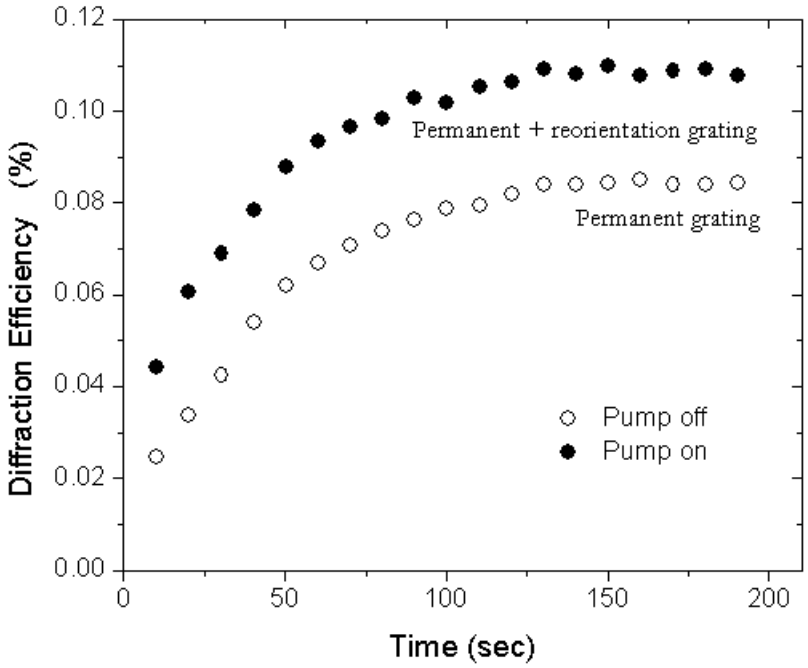

Figure 3.8: Permanent and reorientation grating in 5CB doped with methyl red at 0.3%wt, $1.5mW/cm^2$ [39]

In conclusion, in this work it has been demonstrated that the adsorption of the dye to the substrate of LC can be explained as the contribution of three phenomena: *(i)* the dipole moment, *(ii)* the increase in N=N group charges on dyes with polar groups and *(iii)* the double hydrogen bonding between carboxyl group -COOH in MR and -OH in the substrate. Since no adsorption is observed on MY compared with MR, and -COOH hydrogen bond interaction are stronger compared with N=N interactions, it can be conclude that the polar (acid) group in MR dye plays a very important role on dye adsorption. It has been demonstrated that in addition to N=N interaction, H-bonding interaction facilitates stronger anchoring on the substrate. This study suggests that strong interaction (ionic) will render better anchoring which would result in better grating formation. Finally, MY can be a suitable dye to enhance the nonlinear optical response of the liquid crystals on the blue region of the absorption spectra without the inconvenience of permanent gratings.

3.3 Anisotropy in the diffraction gratings

The diffraction efficiency of a grating recorded in a 5CB-MR 1% doped cell was measured as function of the probe beam's polarization. Since the LC and dye molecules are anisotropic (rod-shape), it is expected that the gratings to be polarization dependent. In randomly oriented sample no polarization effects are expected, but once the grating is recorded they should appear, as it is demostrated in this section. The experimental set-up consists in the pump-probe configuration, where diffraction gratings are recorded by the pump beam. In order to control the probe polarization direction, a $\lambda/2$ waveplate was placed in front of the He-Ne laser (Fig. 3.9).

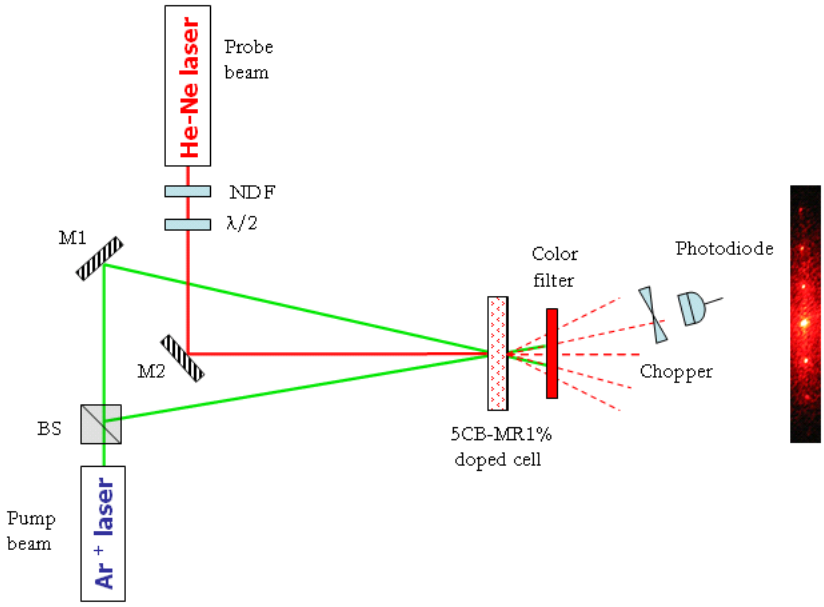

Figure 3.9: Schematic experimental set-up.

3.3.1 Results and discussion

In the dark fringes the molecules remain the random orientation. In contrast, according to Komitov *et. al.* [37], in the bright fringes the molecules tend to adopt perpendicular orientation with respect to the substrate. If this is true, one would

expect not to find a diffraction efficiency dependence on the probe beam polarization. However, in all the measurements a strongly anisotropic behavior was observed, as shown in Fig.3.10. In this figure, $0°$ and $90°$ corresponds to parallel and orthogonal polarization of the probe beam with respect to the pump, respectively. The sinusoidal behavior of the diffraction efficiency suggests that the dye is not perpendicularly anchored to the substrate, and therefore, the LC reorientation induced by the dye is not perpendicular. In addition, it was also found a phase shift in the measurements from sample to sample and from one region to another one in the same sample as shown in Figure 3.10.

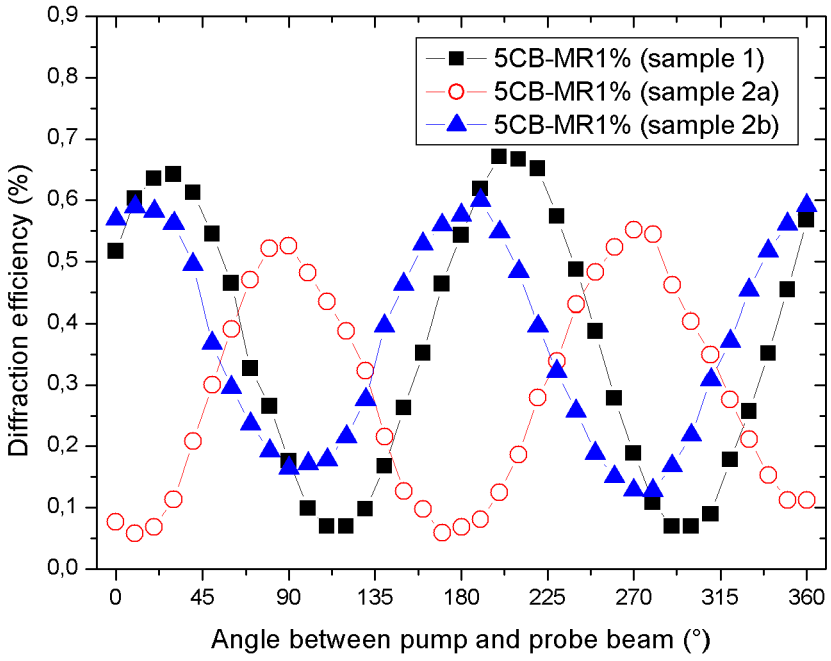

Figure 3.10: Anisotropic response of two samples at the same conditions.

The anisotropy measured in these plots can be attributed to the angle of the dipole moment of the *cis* anchored isomer. The reorientation angle of the molecules seems to have a value large enough to introduce a difference between parallel and orthogonal polarization of the probe beam.

In order to confirm this hypothesis, some numerical simulations were performed to calculate the angle of the dipole moment, and therefore, the reorientation angle of the adjoining LC molecules [58]. The numerical simulations based on the software *PM3 (Molecular mechanics, semi-empirical)* gave an angle of $\sim 55°$ between the dipole moment and the substrate [See Fig.3.11(a)]. As a result, the LC are also aligned in this direction, explaining the strong diffraction efficiency dependence on the probe beam polarization direction but it is not enough argument to explain the phase shift in the curves. Hence, another issue must be considered: since this angle is measured with respect to the substrate, the dipole can have different orientation which is illustrated in Fig. 3.11 (b). Arrows in this figure represent some possible dipole moment orientations keeping the $\sim 55°$ angle.

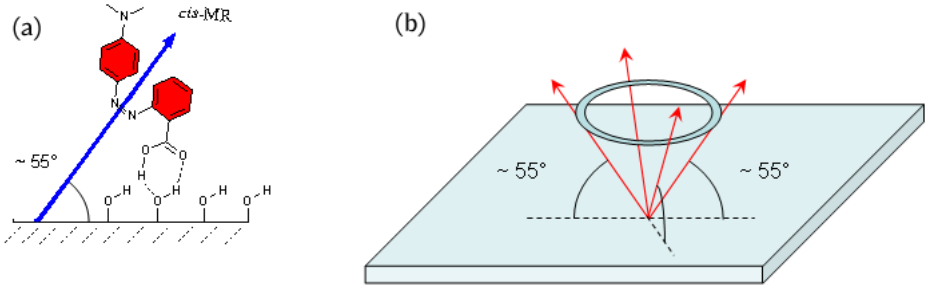

Figure 3.11: Direction of the MR dipole moment anchored on the substrate. (a) The angle with respect to the substrate is $\sim 55°$ (two dimensions). (b) In 3D the *cis*-MR isomer can be anchored with different orientations.

When a diffraction grating is recorded in a dye doped LC sample, the polarization of the pump beam induces a reorientation over the molecules present in the bright fringes. The dark fringes present a random orientation of the dye and LC molecules. Moreover, in the case of the bright fringes, although the angle between the dipole moment and the substrate is the same $(\sim 55°)$ it can have different orientation for different domains in the fringe.Figure 3.12 represents the orientation of the dye anchored dipole moment in a recorded grating. The circles represent the domains of the induced reorientation angle over the liquid crystal molecules.

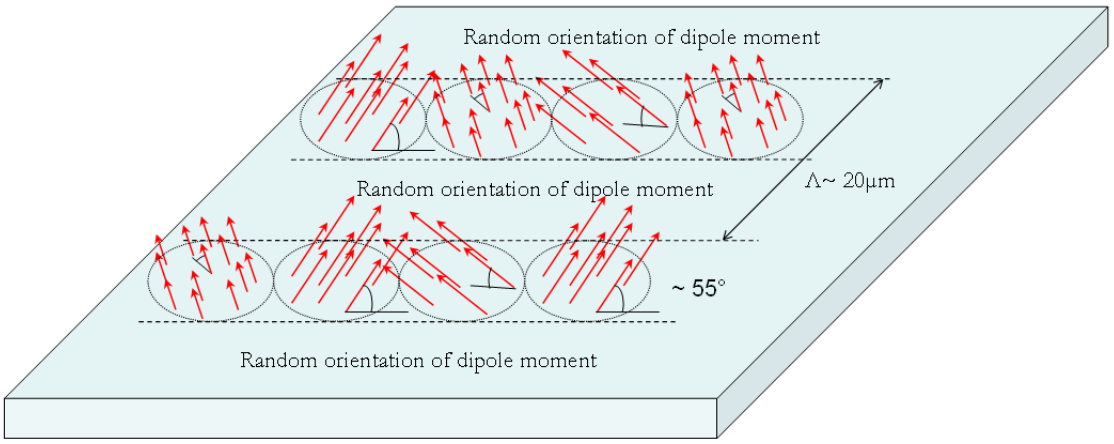

Figure 3.12: Different regions in a permanent grating recorded with period $\Lambda \approx 20\mu m$. Arrows represent the orientation of the dipole moment.

The differences in the dye orientation are manifested in the induced LC orientation. In adittion, taking into account that the illumination area of the probe beam is 6 times smaller than the one for the pump beam, it is possible to measure in any domain of the grating. This means that due to the difference in the orientation for each domain, it is possible to begin the measurements from any value in the curve of anisotropy. Thus, a phase shift in the curves can be found for one region to another one, or from one sample to another one.

3.4 Change polarization due to beam propagation in LC

It is important to measure the change in polarization that a linearly polarized beam suffers after propagation through a DDLC sample. This measurement provides information related with the material anisotropy. In order to do this experiment, a weak linearly polarized He-Ne laser ($10mW/cm^2$) was transmitted through a 5CB-MR1% planar cell. In addition, a $\lambda/2$ waveplate was used to control the polarization of the laser, and one polarizer was placed after the sample to analyze the output polarization state. Fig. 3.13 shows the experimental set-up.

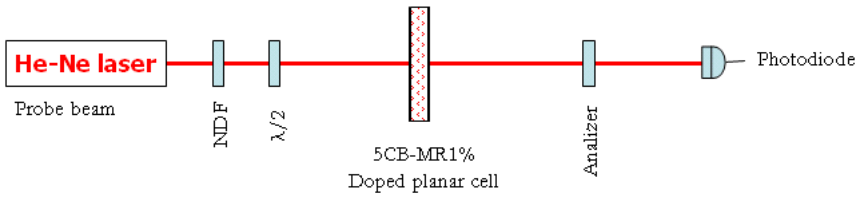

Figure 3.13: Schematic experimental set-up to analyze the change in polarization due to the anisotropic response of a 5CB-MR1% doped planar cell.

3.4.1 Results and discussion

The largest phase shift is expected to be not in the ordinary or extraordinary polarization but at 45° with respect to the director, i.e. both components of the polarization are equal. Figure 3.14 shows the results obtained in this experiment for extraordinary polarization and for polarization at 45° with respect to the director. The material anisotropy is manifested as changes on the output polarization of the probe beam.

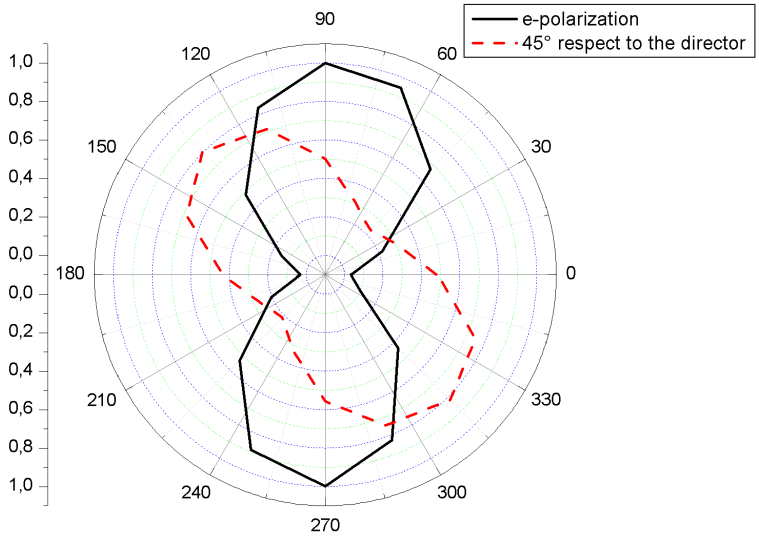

Figure 3.14: Extraordinary and 45° polarization with respect to the molecular director of a planar cell.

For extraordinary input polarization, as expected, the polarization states does not change (linearly polarized). The linear polarization is manifested in the value of zero for the orthogonal components as plotted in the continuous curve in Fig.3.14. On the other hand, for $45°$ polarization, the output changes from linear to elliptic polarization state as observed in the dashed curve in Fig.3.14. The polarization change is observed in the increased of the orthogonal components, while the parallel ones have decreased. The dashed curve presents a $45°$ rotation with respect to the continuous curve, due to the rotation of the polarization illumination. The change in the phase needed to change from linear to elliptic polarization was $0.65rad$ (this calcule considers the phase change due to the waveplate rotation).

3.5 Response and relaxation time

The response and relaxation time in a 5CB-MR1% doped planar cell was measured as function of the pump beam intensity and polarization. The experimental set-up consists in pumping a planar cell with intensities: $53mW/cm^2, 70mW/cm^2, 88mW/cm^2$ and $106mW/cm^2$ with a linearly polarized Ar^+ laser. The polarization of this laser has been controlled by a $\lambda/2$ waveplate in order to achieve extraordinary and ordinary polarization. A weak He-Ne laser with extraordinary polarization was used to probe the response time of the molecules. The experimental set-up is shown in Fig.3.15. For the response time, at a certain time, the pump laser is on and remained in this state until the induced transmittance achieve a steady value. Once this measurement time was registered, the Ar^+ laser was turned off, in order to observe the relaxation time of the sample. The characteristic behavior is shown in the plot in Fig.3.15. The diameter of the probe beam is 6 times smaller that the one for the pump laser. The photodiode signal was processed by a lock-in-amplifier. An integration time was chosen such that the temporal dynamics is not affected by the integration time of the lock-in. Finally, the data were measured and saved in an osciloscope.

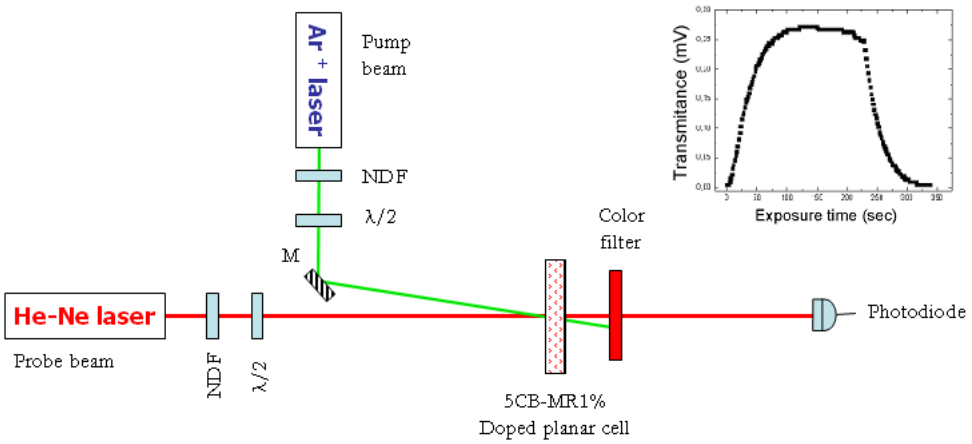

Figure 3.15: Schematic experimental set-up. $\lambda/2$ waveplates are used to control the polarization of both lasers.

3.5.1 Results and discussion

Let us start the discussion with the response of the material when the pump is on. In Figures 3.16 and 3.17 the response time as function of the pump intensity for extraordinary and ordinary polarization are plotted. From these plots it is possible to obtain information related with the transmittance dependence on intensity and polarization.

By taking into consideration Eq.2.28 $\left[X = \frac{X_{sat}}{1+\tau_0/\tau}\right]$ in Section2.1.7.2, where X is the *cis* isomers fraction, X_{sat} is the saturation value of X, τ_0 is the characteristic time for the formation of the steady state *cis* isomers and τ is the exposure time, it is possible to find the values for τ_0. Since X is proportional to the transmittance, the response time can be fitted by using Eq.3.1.

$$T = \frac{T_{sat}}{1 + \tau_0'/\tau}, \tag{3.1}$$

where T is the transmittance, T_{sat} is the saturation value of T, and τ_0' is the response time. It can be observed that this equation canot describe the experimental results for short exposure time, but a good agreement has been achieved for long exposure times. It means that the dynamic in Figs.3.16 and 3.17 includes at least two dif-

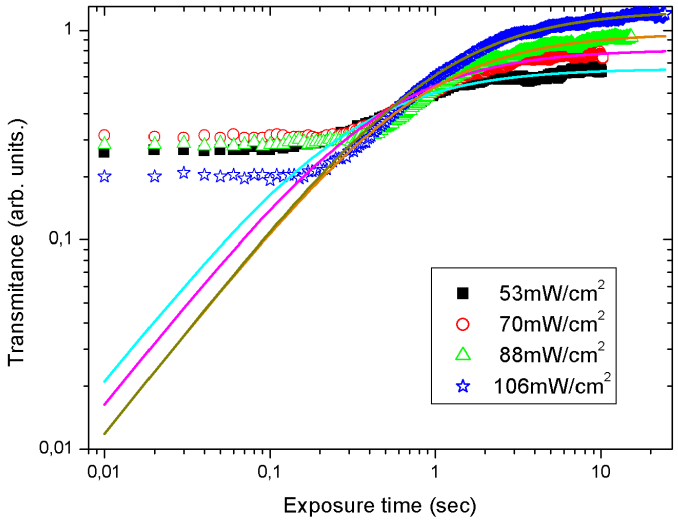

Figure 3.16: Response time for a 5CB-MR1% planar cell with extraordinary polarization of the pump beam. Lines represent the fit to Eq.3.1.

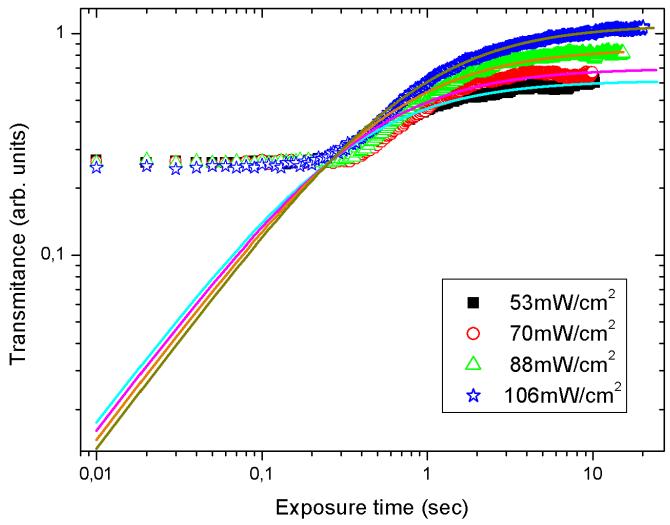

Figure 3.17: Response time for a 5CB-MR1% planar cell with ordinary polarization of the pump beam. Lines represent the fit for Eq.3.1.

ferent processes which will not be disscused since the response time is not issue for our applications. However, more detailed studies are requiered to elucidate other mechanisms thet contribute to the increase of the response time. In the following sections, the transmitance and response and relaxation time are analyzed.

3.5.1.1 Transmittance

The values found for T_{sat} are plotted in Fig.3.18. As expected for the transmittance saturation value, the higher the intensity the higher the value for T_{sat}. It is attributed to the formation of *cis* isomers, which have lower absorption cross-section than the *trans* isomers [59]. For the same reason, since the experiments are carried out in a planar cell, and the probe beam has extraordinary polarization, it is predictable to measure higher transmittance for extraordinary than for ordinary pump intensity, as reported in Fig.3.18.

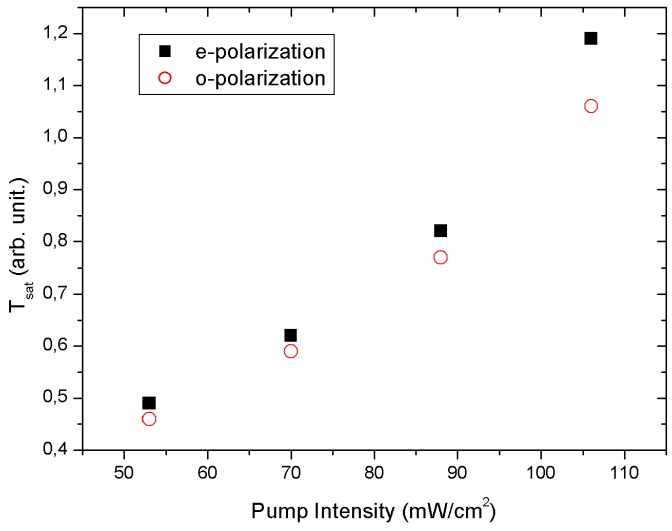

Figure 3.18: Saturation transmittance

As can be observed in Fig.3.18, the values for the transmitance do not reach saturation, but by increasing the pump beam intensity it is posible to achieve saturation values. However, this research is concerned with low power applications, for this reason these measurements were performed under these conditions.

3.5.1.2 Response Time

In Section2.1.7.2 it is stated that τ_0 decreases as the light intensity is increased. However, the result for the fitting of the values in Eq.3.1 shows that τ_0', is increased as the intensity is increased (Fig.3.19). At this point, it is worth mentioning that when the intensity is high enough, other mechanisms may to be considered i.e., dye diffusion and lifetime of excited states [60], increase in the temperature, changes in the order parameter, viscosity, refractive index, among others. In the same idea, taking into account that τ_0 is described by Eq. 2.29 $[1/\tau_0 = p_T\Phi_{TC} + p_C\Phi_{CT}]$ (p_C, p_T, are the *trans* and *cis* excitation probabilities, Φ_{TC} and Φ_{CT} are the quantum efficiencies of the *trans*-*cis* and *cis*-*trans* transitions, respectively), the presence of these mechanisms suggests a competition between the existence of *trans* and *cis* isomers, thus, the values for p_C, p_T, Φ_{TC} and Φ_{CT} are difficult to be estimated.

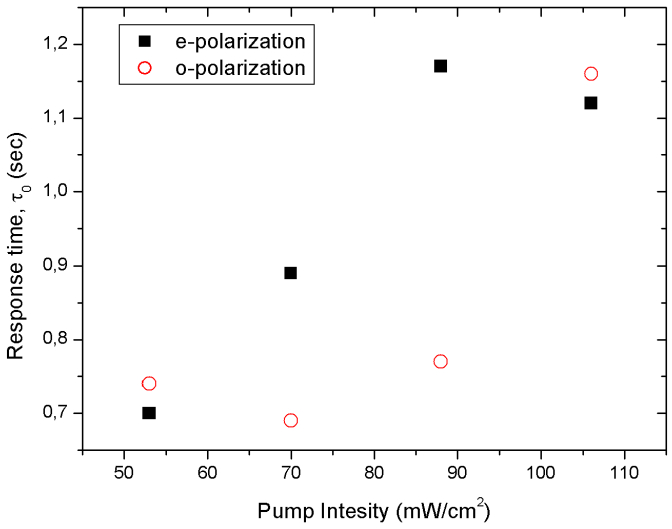

Figure 3.19: Response time

3.5.1.3 Relaxation time

In the case of the relaxation time, the results for extraordinary and ordinary polarization are plotted in Fig.3.20 and 3.21, respectively. As expected, the relaxation

time does not depend on polarization and intensity because in both cases there is no mechanism to obstruct the relaxation back to its original position. Lines in Figs.3.20 and 3.21 represent the fit obtained for an exponential decay function described by Eq.3.2

$$T = \exp -(\tau/\tau_r). \tag{3.2}$$

In this equation T is the transmittance, τ is time en seconds, and τ_r is the relaxation time.

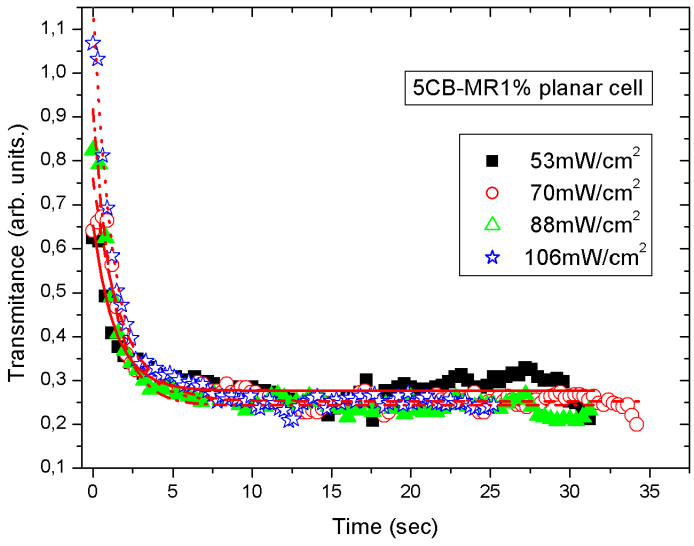

Figure 3.20: Relaxation time for a 5CB-MR1% doped planar cell as function of intensity and for extraordinary pump polarization.

The obtained values for τ_r are plotted in Fig.3.22. The mean value is $1.29sec$, and from Fig.3.22 it is possible to observe that this value remains constant.

The relaxation time values reported for 5CB are between $(20 - 100msec)$ for any intensity level [60], however, it has been proven that dye diffusion and life time of the excited states have to be considered. For the purpose of this thesis a detailed study of the response and relaxation time is not relevant, but it is an important parameter

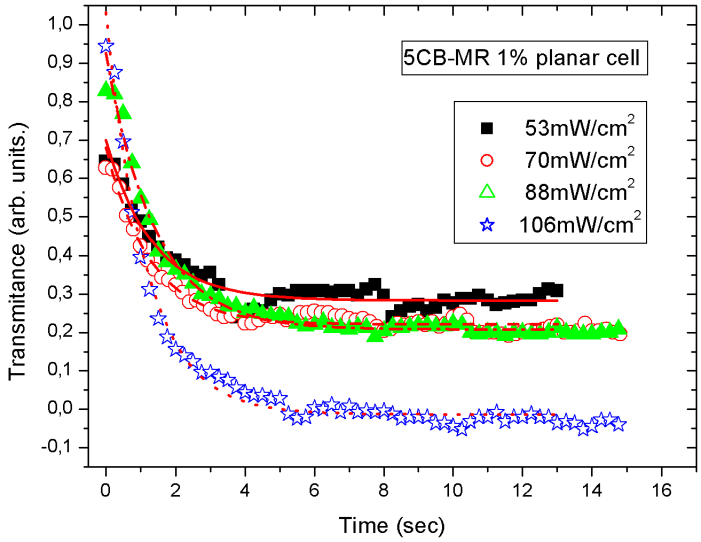

Figure 3.21: Relaxation time for a 5CB-MR1% doped planar cell as function of intensity and for ordinary pump polarization.

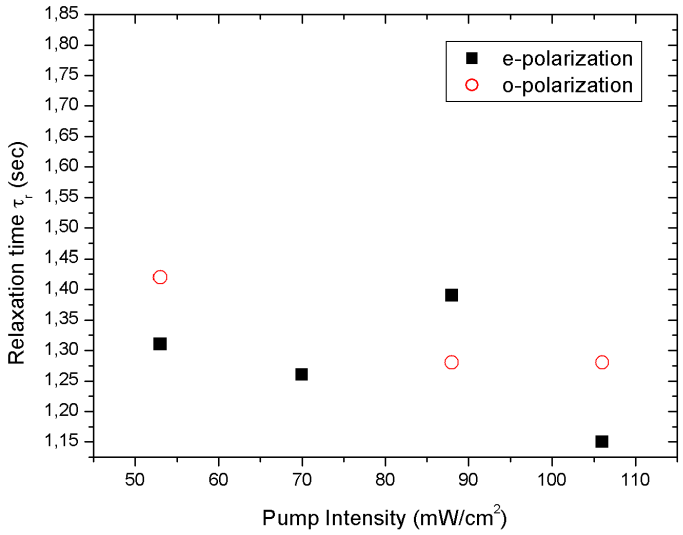

Figure 3.22: Relaxation time

that needs to be analyzed more carefully, in order to elucidate other reorientation mechanisms.

3.6 Cis fraction measurements

The goal of this experiment is to determine the relation between the phase change induced by a 5CB+MR1% doped planar cell, as function of the polarization's illumination. This relation has relevant importance in the phase contrast experiments, where this dependence is exploited.

Equation 2.36, describes the relation of the ratio (X_S/X_{ord}) as function of Ψ, $(X_S/X_{ord} = \frac{1+g\cos^2\Psi}{1+h\cos^2\Psi})$, where X_S is the fraction of *cis* isomers. Ψ is the angle between the direction of polarization light and the molecular director, X_{ord} is the fraction of *cis* isomers for ordinary polarization, and g and h are molecular parameters different for each LC doped system. Based on the Janossy model [33], it is possible to find g and h, by performing transmittance measurements (detailed in Eqs.2.44). The relation between these measurements and X_S/X_{ord} is given by expression 2.45:

$$X_S/X_{ord} = \frac{\ln T_S/T_T}{\ln T_{ord}/T_T},$$

where T_T is the transmittance for a sample with the dye in the *trans* isomer, T_S and T_{ord} are the transmittances for the extraordinary and ordinary polarized beam, respectively. By considering X_S and T_S the corresponding values for different angles Ψ from extraordinary to ordinary polarization, X_S and T_S become X and T. Thus Eq.2.45 can be expressed as:

$$X/X_{ord} = \frac{\ln T/T_T}{\ln T_{ord}/T_T}, \tag{3.3}$$

For this experiment a He-Ne laser $(633nm)$ was employed to illuminate a 5CB-MR1% doped planar cell. The transmittance was obtained by sensing the power before and after the sample, (T_{out}/T_{in}). In order to find the transmittance for the *trans* state T_T, a weak intensity of illumination was used (this value is expected to be a constant). In order to achieve intensities above the saturation value ($\sim 2.5X10^5 W/cm^2$ at $633nm$), the transmittances for the *cis* state T were measured by focusing the laser with a lens. In addition, the angle Ψ was controlled by rotating a $\lambda/2$ waveplate.

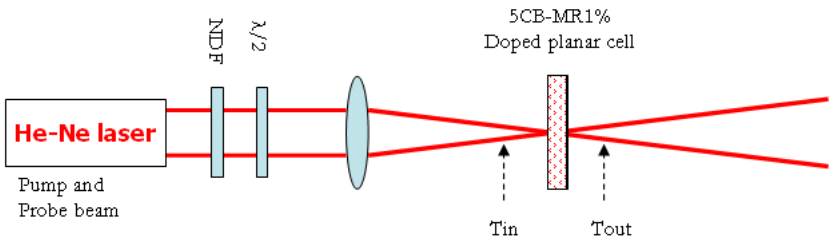

Figure 3.23: Schematic experimental set-up to obtain g and h parameters of the sample.

3.6.1 Results and discussion

Figure 3.24 shows the results obtained in this experiment. X/X_{ord} is plotted as function of $\cos^2\Psi$. The values for T/T_T and for X/X_{ord} are in the same range than in the results obtained by Janossy and Szabados in Ref. [33]. The best fit gives as result the parameters $g = 8.9$ and $h = -0.39$. The line plotted in Fig.3.24 shows this fit.

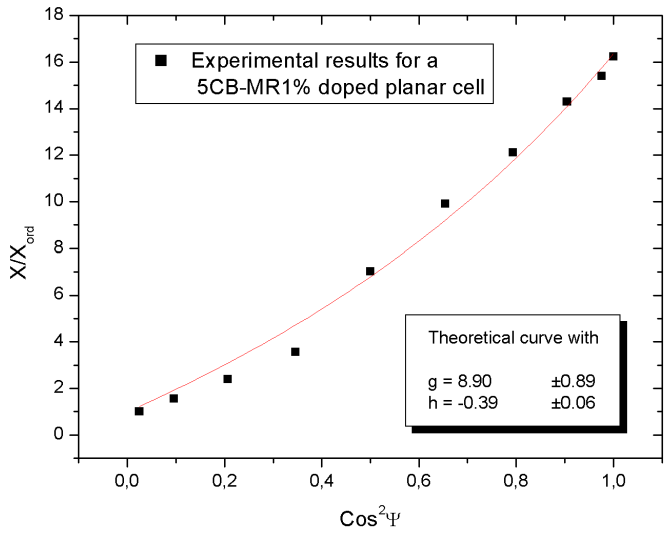

Figure 3.24: Experimental and theoretical results for X/X_{ord} to obtain g and h parameters of the sample.

Unfortunately, since Eq.3.3 includes logarithmic functions, therefore, small changes in T can lead to important differences in the numerical analysis. In spite of this, consistently, we obtained a g value at least 20 times larger than h It allows the employment of the approximation made in Ref. [61]. This approximation is based on two facts: (i) the difference in the values for g and h, and (ii) the dependence of the effective phase change with the input polarization which can be assumed as

$$\Delta\Phi = X\Delta\Phi_N + (1 - X)\Delta\Phi_P, \tag{3.4}$$

where $\Delta\Phi_N$ and $\Delta\Phi_P$ are the phase changes for extraordinary and ordinary polarizations, respectively. By considering this information the effective phase change can be approximated to

$$\Delta\Phi \approx \cos^2\Psi\Delta\Phi_N + \sin^2\Psi\Delta\Phi_P. \tag{3.5}$$

3.7 Conclusions

One of the goals of these experiments was to understand the molecular mechanisms involved in the anchoring of dye molecule to the substrate. So far, it is possible to explain that the there are three reasons for the dye to be anchored in the substrate upon illumination. It has been demonstrated that carboxyl group in MR plays a crucial role in this anchoring, in combination with the increased of the charges of the azo group in the molecule and with the induced dipole moment. It has been also probed that the angle between the substrate and the dipole moment causes the anisotropic dependence on the diffracted beam. In addition, it has been observed that the liquid crystal sample can change the polarization state a polarized illumination beam in function of intensity and of the angle between the molecular director and the polarization of the beam. From the response and relaxation time experiments, it can be concluded that the response time of the material is $\sim 0.7sec$ at $53mW/cm^2$ and the relaxation time is $\sim 1.36sec$. Finally, The g and h parameters have been found as function of the angle

between polarization and the molecular director. These information is important in order to achieve the second major objective of this research work: to implement a phase contrast microscope using a dye doped liquid crystal planar cell as a nonlinear filter. In the following chapter this subject is described in detail. The experiments and results of the quantified contrast for different phase objects are reported and the implementation in real-time is demonstrated.

Chapter 4

Phase contrast microscopy by dye-doped liquid crystals

4.1 Introduction

It is well known that light propagation in Kerr-type nonlinear material modifies its refractive index [62]. The change in refractive index scales linearly with the illumination intensity and can be positive or negative depending on the material's characteristics. If a nonlinear material is placed at the Fourier plane of the optical system, then the Fourier intensity distribution generates an apodized phase filter. In order to achieve the Zernike filter by using a nonlinear material and with the minimal distortion in the contrasted images, it is desirable that the photoinduced filter alters only the phase of the zero frequency components and some small vicinity around it [63]. This is accomplished by assuming a phase object whose Fourier-transform has its maximum intensity at the zero frequency and the intensity of the higher frequency components is much weaker [fill factor < 1, (see Section 2.2.2)]. A consequence of this type of filtering is that the maximum contrast is slightly reduced compared to the one obtained with classical Zernike filtering. Nevertheless, nonlinear filtering offer several advantages since it does not suffer from fabrication or alignment difficulties, with the exception of its placement at the adequate plane in the optical system. However, in order to make the filter attractive, other important characteristics must also be

fulfilled. Such characteristics include fast response time (at least video frame rates should be attainable), high sensitivity, high spatial resolution, operation with relatively low power light sources, and low cost.

As mentioned before, dye-doped nematic liquid crystals (DDNLC) offers several promising characteristics to be considered as nonlinear filter. Its colossal nonlinearity [1] its dependence on applied field [8], temperature [10] and dye dopants make of this material probably the best candidate for phase contrast. LC's possess an important property which makes them suitable to be used as a Zernike filter: to be reorientated, the molecules need a certain level of intensity threshold (Fredericz's transition [27]), otherwise, the change in the refractive index is not induced. This means that, if the fill factor requirements are achieved and the intensity is not in the saturation level, it is possible to induce the Zernike filter in the nonlinear material only in regions where the intensity exceeds the reorientation threshold.

In addition, azo-dye *trans-cis* molecular transitions are responsible for the nonlinear optical increase on the photoinduced torque [7] and, thus, on the enhancement factor of its nonlinear properties(see Section 2.1.7.2). One of the most outstanding characteristics of DDNLC that has to be considered, is its polarization dependent enhancement factor of the optical torque. In fact, it has been proved that the enhancement factor can be changed from positive to negative by changing the relative populations of *trans* and *cis* transitions [33]. Fortunately, the *trans-cis* equilibrium can be controlled by changing the intensity and polarization of the illumination beam at a given wavelength [35]. Therefore, the use of a nonlinear material as DDNLC offers the advantage of controlling the nonlinear response in a large range through polarization.

4.2 Experimental results

The experimental set-up used to visualize microscopic objects is shown in Fig. 4.1. The beam from a linearly polarized He-Ne laser ($\lambda = 633nm$) was employed as the illuminating source. In order to control the power and polarization of the beam, a variable neutral density filter and a $\lambda/2$ waveplate, respectively, were used. The body

of a microscope with a $20X$ objective and a $10X$ ocular was employed to produce a $200X$ magnification imaging system. A planar methyl red doped liquid crystal cell was placed at the Fourier plane of the input image. A CCD camera was used to capture the contrasted images.

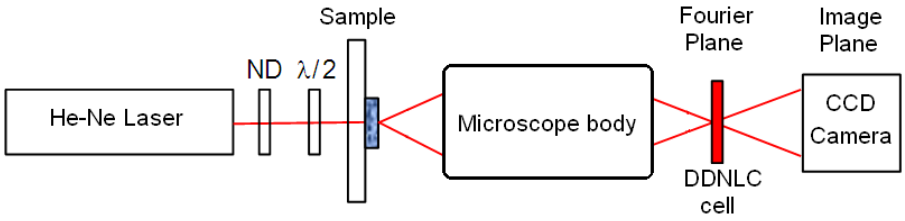

Figure 4.1: Experimental set-up for the phase contrast microscope. DDLC is the dye doped liquid crystal cell.

In order to determine the operational range of our phase contrast microscope, several phase objects were etched on glass plates $(n = 1.5)$. The objects were squares pools of $100\text{x}100\mu m^2$ and different depths $(\lambda, \lambda/2, \lambda/4, \lambda/8, \lambda/20$ and $\lambda/40$, where $\lambda = 633nm)$. As an example, Fig. 4.2 shows the phase contrasted images for the $\lambda/2$ depth square which has a phase difference of $0.5\pi\ rad$. The contrast was measured from the images following the expression $C = (A_i - A_o)/(A_i + A_o)$ where A_i and A_o represents the average intensity values inside and outside the square, respectively. The number on the figures indicates the angle between the rubbing direction and polarization vector. For $0°$ polarization (negative nonlinearity) the phase object looks bright with a dark background. For $70°$ the contrast practically disappears and only the borders of the object are clearly visible, while for $90°$ (positive nonlinearity) the contrast of the image is reversed.

Contrast inversion was observed for all incident powers, as it is shown in Fig.4.3. It can be observed that, due to the competition between the positive and negative nonlinearity, for an angle of almost $70°$ the contrast obtained was very low which is consistent with the Z-scan measurements reported in Ref. [14] and detailed in Section 2.1.8.2.

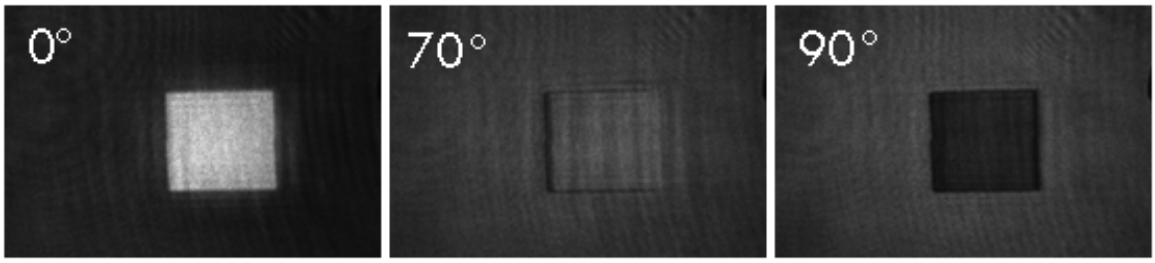

Figure 4.2: Contrasted image of $100x100\mu m^2$ objects etched on glass with a depth of $320nm(\sim \lambda/2)$. The numbers on the top left corner corresponds to the angle between the rubbing direction and the polarization vector of the laser beam. For negative nonlinearity the object is bright on a dark background, for an intermediate angle of $70°$ the contrast almost disappears while for positive nonlinearity the contrast is reversed.

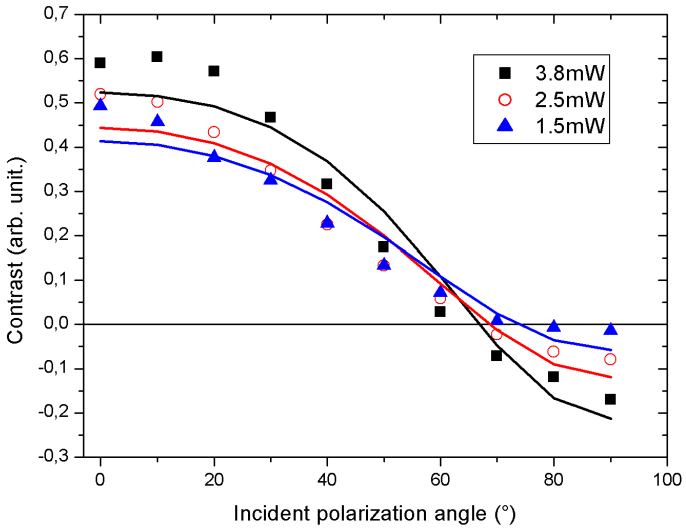

Figure 4.3: Contrast as function of the polarization of the incident beam for different input powers of: 3.8, 2.54 and 1.52 mW for a phase object of $\lambda/2$ thickness. Continuous lines represent fit to the contrast for the same power level.

In Ref. [61] it was shown that the $\Delta\Phi_{E,O}$ dependence on power scales quadratically. In Fig.4.4 the photoinduced phase $\Delta\Phi_T$ in the DDNLC sample is plotted for $0°$ and $90°$ polarization as function of the incident power.

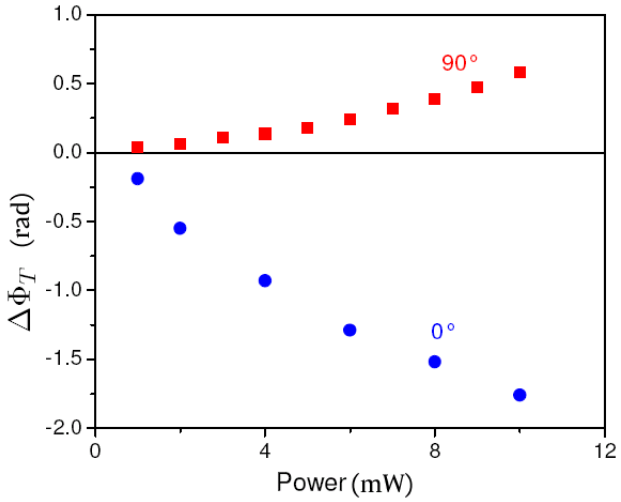

Figure 4.4: Photoinduced phase change for $0°$ and $90°$ polarization as function of the incident power. Taken from Ref.[63].

Since the refractive index depends on intensity and the experimental results reported in Ref. [61] were calculated for incident power at different conditions, it is not possible to compare them with the induced phase change in the phase contrast experimental results.

4.2.1 Edge enhancement

It was been found that for a phase change of 4.8π in the object, it is possible to observe edge enhancement in the resulting image. Figures 4.5 shows the image for ordinary and extraordinary polarization. The edge contrast depends on intensity, however even with low illumination power it is possible to observe it. So far, our theoretical model can not reproduce these results. Therefore, this subject will be object of a detailed analysis in a future work.

4.2.2 Real-time applications

The proposed system can be used to visualize phase objects where contrast of the images can be changed in order to enhance different components of the image. Biological samples may contain objects with spatially changing phases, and hence

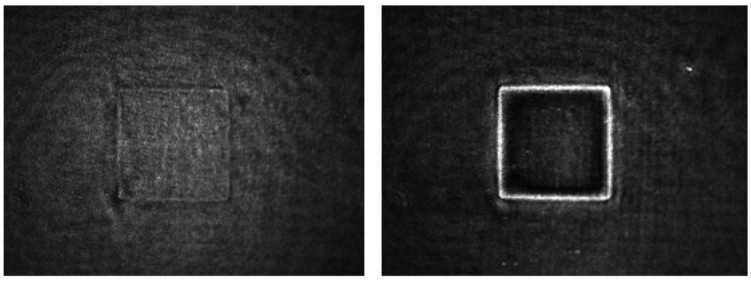

Figure 4.5: Image for the binary phase mask ($\Delta\varphi \approx 4.8\pi$) for ordinary polarization. Edge enhancement for the binary phase mask ($\Delta\varphi \approx 4.8\pi$) for extraordinary polarization.

they are good candidates to demonstrate the performance of the system with dynamic events. Fig.4.6, shows some biological specimens (*Paramecium, a unicellular ciliate protozoa*) observed under the nonlinear phase contrast microscope. These images have been obtained in real time and rotating the $\lambda/2$ plate. It can be observed that the contrast can be adjusted in real time to observe some specific detail in the phase objects.

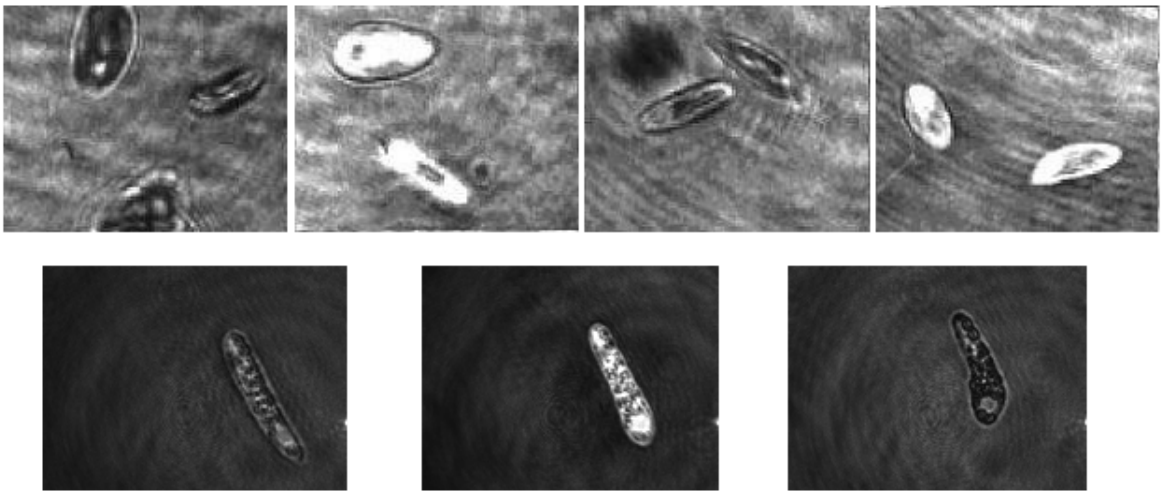

Figure 4.6: Real time images of biological specimens (*paramecium*) obtained by the nonlinear phase microscope. The $\lambda/2$ plate was rotated in order to improve the contrast. The size of the living organisms is $\sim 75\mu m$ long.

4.3 Conclusions

In this research work it has been demonstrated the outstanding performance of a liquid crystal 5CB methyl red doped planar cell as a nonlinear phase filter in a phase contrast image system. The phase of such filter, for illumination at $633nm$, can be switched from positive to negative by changing the incident polarization respect to the cell director vector and its magnitude can be controlled with the incident power.

In addition, real time operation offered by this technique allows the tuning of the image contrast in dynamic visualization of living organisms. It has been also observed an inversion in the contrast for a binary phase object and in microorganisms. The phase contrast proposed in this work can be easily implemented in standard microscopes without further complications.

Chapter 5

General Discussion and Outlook

5.1 Summary

This dissertation reported the results of nonlinear optical studies carried out on dye-doped nematic liquid crystal cells. The major contribution of this thesis was the application of the nonlinear optical properties of LC in image processing. In particular, the refractive index dependence on polarization was satisfactory applied in phase contrast microscopy.

The first part of the results in this thesis concerns with the characterization of the dye doped liquid crystal, the information obtained from this research is given in the following lines.

The permanent diffraction grating formation in methyl red azo dye doped liquid crystal cells was studied using a pump-probe configuration. The experimental results obtained with the comparison of methyl red and methyl yellow and the numerical simulations show that the double hydrogen bonding between carboxyl group -COOH in methyl and -OH in the substrate has an enormous contribution in the photoadsorption of the dye to the substrate. This effect combined with the change in the dipole moment and the increased in N=N group charges on dyes with polar groups explain the dye anchoring in the cells.

It was also proven that the angle between the dipole moment and the substrate is $\sim 55^{\circ}$ and plays and important role in the induced reorientation of the LC molecules,

since the diffraction efficiency of the recorded gratings showed a strong dependence on the polarization's probe beam.

In addition, a dye doped liquid crystal cell with planar alignment was illuminated with a linearly polarized beam in order to find the change on the polarization state for low intensities. The results show that a $45°$ linearly polarized beam turns to elliptic polarization after propagation through the cell (phase change of $0.65rad$).

On the other hand, the dynamic observed during the experiments shows that the model described for this mechanism need to take into consideration other mechanisms i.e. dye diffusion, life time of excited states, increase in the temperature, changes in the order parameter, viscosity, refractive index, among others. Since the aim of this work is not related with this issue, it will be carefully studied in a future work in order to clarify the process.

In relation to the phase change dependent on intensity and polarization's beam, an approximated equation was given. Transmittance measurements were performed in order to obtain the g and h molecular parameters which describe the relation between the fraction of *cis* isomers and the angle of polarization. The approximated equation is based on the assumption that g is at least 20 times larger than h and on the fact that the dependence of the effective phase change with respect to the polarization can be expressed as $(\Delta\Phi = X\Delta\Phi_N + (1-X)\Delta\Phi_P)$ [61].

Polarization controlled contrasted images were acquired by using a dye-doped nematic liquid crystal cell with planar alignment as a nonlinear filter. The images obtained showed that the refractive index change can be switched from positive to negative one as the polarization's beam changes from extraordinary to ordinary direction. In addition, the model for the image contrast describes properly the contrast measured for the experimental results. These results include the contrast for known phase objects and for different illumination power, where inversion in the contrast was observed. The smallest phase change measured was for the object of $\lambda/8$ at $633nm$, but its is possible to obtain a higher performance since the limitation is related with the quality of the fabrication cell, which can be improved.

Finally, it was possible to acquire real-time images of living microorganisms. The contrast of these images was controlled by rotating the angle of polarization's beam and inversion in the contrast was observed.

5.2 Future work

As mentioned before, the response and relaxation time of the dye doped liquid crystals need to be detaily studied in order to clarify the mechanisms which take place upon illumination.

It is also important the characterization of the state polarization induced by a dye doped liquid crystal in the nonlinear regime. This information is useful to study the state polarization of the images acquired by the phase contrast system.

The fabrication of the planar liquid crystal cells need to be improved in order to obtain higher quality in the contrasted images.

Finally, in relation to the edge enhancement observed for objects with change phase of $\sim 4.8\pi rad$, a careful analysis is needed to elucidate the process which makes possible this effect.

Bibliography

[1] L. Lucchetti, M. Di Fabrizio, O. Francescangeli, and F. Simoni. Colossal optical nonlinearity in dye doped liquid crystals. *Opt. Comm.*, 233:417–424, 2004.

[2] L.I. Olivos Perez, M.D. Iturbe Catillo, D. Sanchez de la Llave, R. Ramos-García, , and C.G. Treviño-Palacios. Nonlinear phase contrast microscope. *Proc. of SPIE*, 6332:633210–1 – 633210–8, 2006.

[3] L. Marrucci. Mechanisms of giant optical nonlinearity in light-absorbing liquid crystals: a brief primer. *Liq. Cryst. Today.*, 11:1–28, 2002.

[4] I. C. Khoo, J. Ding, A. Diaz, Y. Zhang, and K. Chen. Recent Studies of Optical Limiting, Image Processing and Near-Infrared Nonlinear Optics with Nematic Liquid Crystals. *Mol. Cryst. Liq. Cryst.*, 375:33–44, 2002.

[5] P. J. Collings and M. Hird. *Introduction to liquid crystals: Chemistry and physics*. Taylor & Francis, Bristol, 1997.

[6] B.Y. Zeldovich, N.F. Pilipetski, A.V. Sukhov, and N.V. Tabiryan. Giant optical nonlinearity of a nematic liquid crystal. *JETP Lett.*, 31:264, 1980.

[7] I. Janossy, A.D. Lloyd, and B.S. Wherret. Anomalous optical freedericksz transition in absorbing liquid crystal. *Mol. Cryst. Liq. Cryst.*, 179:1, 1990.

[8] I.C. Khoo, S. Slussarenko, B.D. Guenther, M.Y. Shih, P.H. Chen, and W.V. Wood. Optically induced space-charge fields, dc voltages, and extraordinarily large nonlinearity in dye-doped nematic liquid crystals. *Opt. Lett.*, 23:253–255, 1998.

[9] I.C. Khoo, M.V. Wood, M.Y. Shih, and P.H. Chen. Extremely nonlinear photosensitive liquid crystals for image sensing and sensor protection. *Opt. Expr.*, 4:432, 1999.

[10] R. Ramos-Garcia, I. Lazo-Martinez, I. Guizar-Iturbide, A. Sanchez-Castillo, M. Boffety, and P. Ruck. Linear and nonlinear optical properties of photochromatic molecules and materials. *Chem. Rev.*, 100:1817–1846, 2000.

[11] W. M. Gibbons, P. J. Shannon, S. T. Sun, and B. J. Swetlin. Surface-mediate alignment of nematic liquid crystals with polarized laser light. *Nature*, 351:49–50, 1991.

[12] Nobel Prize. Frits Zernike - biography. `nobelprize.org`.

[13] I. Janossy. Optical reorientation in dye-doped liquid crystals. *Journal of Nonlinear Optical Physics and Materials*, 8:361–377, 1999.

[14] A. Rodriguez-Rosales, R. Ortega-Martinez, L. Arroyo Carrasco, E. Reynoso Lara, C. Trevino Palacios, O. Baldovino-Pantaleon, R. Ramos Garcia, and M. D. Iturbe-Castillo. Neither kerr nor thermal nonlinear response of dye doped liquid crystal characterized by the z-scan technique. *Mol. Cryst. Liq. Cryst.*, 489:335–347, 2008.

[15] S. Chandrasekhar. *Liquid Crystals - Second edición.* Cambridge University Press, Great Britain, 1994.

[16] F. Simoni and O. Francescangeli. Effects of light on molecular orientation of liquid crystals. *J. Phys.: Condens. Matter*, 11:R439–R487, 1999.

[17] I. C. Khoo. *Liquid Crystals: Physical properties and nonlinaer optical phenomena - 4th edition.* John Wiley & Sons, USA, 1995.

[18] P. J. Collings. *Liquid Crystals, Nature's Delicated Phase of Matter - Second Edition.* Princeton University Press, USA, 2002.

[19] S. Singh. *Liquid Crystals Fundamentals.* World Scientific, Singapore, 2002.

[20] M. Born and E. Wolf. *Principles of Optics, 6th edition*. Pergamon Press, Headington Hill Hall, England, 1980.

[21] A. Yariv and P. Yeh. *Optical Waves in Crystals, Propagation and Control of Lares Radiation*. Wiley, Hoboken, New Jersey, 2003.

[22] S. McConville, D. Laurent, A. Guarino, and S. Residori. Measurements of the giant nonlinear response of dye-doped liquid crystals. *Am. J. Phys.*, 73:425–432, 2005.

[23] N.V. Tabiryan, A.V. Sukhov, and B.Y. Zeldovich. Orientational optical nonlinearity of liquid crystals. *Mol. Crys. Liq. Cryst.*, 136:1–139, 1986.

[24] I. Janossy and A.D. Lloyd. Low-power optical reorientation in dyed nematics. *Mol. Cryst. Liq. Cryst.*, 203:77, 1991.

[25] Y. R. Shen. *The Principles of Nonlinear Optics*. Wiley, New York, USA, 1984.

[26] E. Hecht. *Optica - Third edition*. Addison Wesley Iberoamerica, Madrid, Spain, 2000.

[27] F. Simoni, O. Francescangeli, Y. Reznikov, , and S. Slussarenko. Dye-doped liquid crystals as high-resolution recording media. *Opt. Lett.*, 22:549–551, 1997.

[28] P.G. de Gennes and J. Prost. *The Physics of Liquid Crystals*. Oxford Universtity, 2001.

[29] F. Simoni. *Nonlinear Optical Properties of Liquid Crystals and Polymer Dispersed Liquid Crystals*. World Scientific, Singapore, 1997.

[30] I. Janossy and T. Kosa. Influence of anthraquinone dyes on optical reorientation of nematic liquid crystals. *Opt. Letters*, 17:1183–1185, 1992.

[31] L.M. Blinov. Photoinduced molecular reorientation in polymers, langmuir-blodgett film sand liquid crystals. *J. Nonlinear Opt. Phys. Mat.*, 5:165, 1996.

[32] E. Santamato, G. Abbate, P. Magdalena, L. Marrucci, D. Paparo, and E Massera. Optical reorientation in dye-doped nematics. *Mol. Cryst. Liq. Cryst.*, 302:111–120, 1997.

[33] I. Janossy and L. Szabados. Optical reorientation of nematic liquid crystals in the presence of photoisomerization. *Physical Review E*, 58:4598–4604, 1998.

[34] J. A. Delaire and K. Nakatani. Linear and nonlinear optical properties of photochromatic molecules and materials. *Chem. Rev.*, 100:1817–1846, 2000.

[35] I. Janossy and L. Szabados. Photoisomerization of azo-dyes in nematic liquid crystals. *Journal of Nonlinear Optical Physics and Materials*, 7:539–551, 1998.

[36] D. L. Ross and J. Blanc. *Photochroismism, Techniques of Chemistry, Brown*. Wiley-Interscience, New York, USA, 1971.

[37] L. Komitov, K. Ichimura, and A. Strigazzi. Light-induced anchoring transition in a 4,4'-disubstituted azobenzene nematic liquid crystal. *Liq. Cryst.*, 27:51–55, 2000.

[38] L. Komitov, C. Ruslim, Y. Matsuzawa, and K. Ichimura. Photoinduced anchoring transitions in a nematic doped with azo dyes. *Liq. Cryst.*, 27:1011–1016, 2000.

[39] O. Baldovino-Pantaleon, R. Porras-Aguilar, and R. Ramos-Garcia. Anchoring on ito and glass substrates using 4-dimethyl-amino substituted azobenzene dyes doped liquid crystals. *Mol. Crys. Liq. Crys.*, 488:1–10, 2008.

[40] M. I. Barnik, A. S. Zolot'ko, and V. F. Kitaeva. Interaction of light with a dye doped nematic liquid crystal. *JETP*, 84:1122–1130, 1997.

[41] Wei Lee, Hui-Yui Chen, and Sheng-Long Weh. Surface sustained permanent gratings in nematic liquid crystals doped with carbon nanotubes. *Optics Express*, 10:482, 2002.

[42] A. Yariv and P. Yeh. *Optical Waves in Crystals*. Wiley, Hoboken, NJ, 2003.

[43] E. W. Van Stryland and M. Sheik-Bahae. *In Characterization Techniques and Tabulations for Organic Nonlinear Materials*. Marcel Dekker Inc., USA, 1998.

[44] F. Zernike. Diffraction theory of knife-edge test and its improved form, the phase contrast. *Not. R. Astron. Soc.*, 94:371, 1934.

[45] F. Zernike. How I Discovered Phase Contrast. *Science*, 121:345–349, 1955.

[46] J. W. Goodman. *Introduction to Fourier Optics - Third edition*. Roberts & Company Publishers, USA, 2005.

[47] C. G. Trevino Palacios, M. D. Iturbe Castillo, and D. Sanchez de la Llave. *Nonlinear phase constrast. In Some topics of modern optics: Contribution to the world in CIOs 25 years of life. Edited by R. Rodriguez Vera and F. Mendoza Santoyo*. Rinton Press, USA, 2008.

[48] M. D. Iturbe Castillo, D. Sánchez de-la Llave, R. Ramos García, L. Olivos-Pérez, L. A. González, and M. Rodríguez-Ortiz. Real-time self-induced nonlinear optical zernike-type filter in a bacteriorhodopsin film. *Opt. Eng.*, 40:2367–2368, 2003.

[49] J. Gluckstad and P. C. Mogensen. Optimal phase contrast in cpi. *Appl. Opt.*, 40:268, 2001.

[50] L. Marrucci and D. Paparo. Photoinduced molecular reorientation of absorbing liquid crystals. *Phys Rev. E.*, 56:1765–1772, 1997.

[51] I. M. Kolthoff. *Acid Base Indicators*. Read Bokks, New York, USA, 2007.

[52] D. M. Walba, C. A. Liberko, E. Korblova, M. Farrow, T. E. Furtak, B. C. Chow, D. K. Schwartz, A. S. Freeman, K. Douglas, S. D. Williams, A. F. Klittnick, and N. A. Clark. Self-assembled monolayers for liquid crystal alignament: simple preparation on glass using alkyltrialkoxysilanes. *Liq. Cryst.*, 31:481–489, 2004.

[53] M. Kaczmarek, M. Y. Shih, R. S. Cudney, and I. C. Khoo. Electrically tunable, optically induced dynamic and permanentgratings in dye-doped liquid crystals. *IEEE J. Quantum Electron*, 38:451–457, 2002.

[54] E. Ouskova, Yu. Reznikov, S.V. Shiyanovskii, L. Su, J.L. West, O.V. Kuksenok, O. Francescangeli, and F. Simoni. Photo-orientation of liquid crystals due to light-induced desorption and adsorption of dye molecules on an aligning surface. *Phys. Rev. E*, 64(5):051709, 2001.

[55] C. B. Aakeroy and K. R. Seddon. The hydrogen bond and crystal engineering. *Chem. Soc. Rev.*, 22:397–407, 1993.

[56] G. R. Desiraju. *Crystal Engineering: The Design of organic Solids*. Elsevier Scientific Publishers, Amsterdam, The Netherlands, 1989.

[57] M. Bohnet. *Ullmann's Encyclopedia of Industrial Chemistry - 6th Edition*. Wiley-VCH, Verlag GmbH & Co. KgaA, Weinheim, 2003.

[58] E. Gonzalez. Numerical simulations of isomerization of methyl red dye molecules. Personal communication.

[59] M. Becchi, I. Janossy, S. Rao, and D. Statman. Anomalous intensity dependence of optical reorientation in azo dye-doped nematic liquid crystals. *Phys. Rev. E*, 69:051707/1–6, 2004.

[60] O. Trushkevych, N. Collins, W. A. Crossland, T. D. Wilkinson, and W. I. Milne. Dynamics in dye-doped lc systems in presence of trans-cis isomerism. *Mol. Cryst. Liq. Cryst.*, 478:221/977, 2007.

[61] R. Porras-Aguilar, J.C. Ramirez-San-Juan, O. Baldovino-Pantaleón, D. May-Arrioja, M. L. Arroyo Carrasco, M.D. Iturbe Castillo, D. Sánchez de-la Llave, and R. Ramos-Garcia. Polarization-controlled contrasted images using dye-doped nematic liquid crystals. *Optics Express*, 17:3417–3423, 2009.

[62] R. L. Sutherland. *Handbook of Nonlinear Optics - Second edition*. Marcel Dekker, Inc., New York, USA, 2003.

[63] C. Trevino-Palacios, M. D. Iturbe-Castillo, D. Sanchez de-la Llave, R. Ramos-Garcia, and L. I. Olivos-Perez. Nonlinear common-path interferometer: an image processor. *Applied Optics*, 42:5091–5095, 2005.